Illinois Center for Advanced Studies of the Universe

NSF/MUSES, grant no OAC-2103680.

Location of the Critical Point from Holography

muses

Jorge Noronha

The QCD Critical Point: Are We There Yet?

October 27, 2025 - November 7, 2025

INSTITUTE for NUCLEAR THEORY

What is the holographic duality?

Maldacena, 1997; Witten, 1998, Gubser, Polyakov, Klebanov, 1998

“Calculations in strongly coupled plasmas using black holes”

Strongly coupled non-Abelian plasma

Classical gravity in d>4

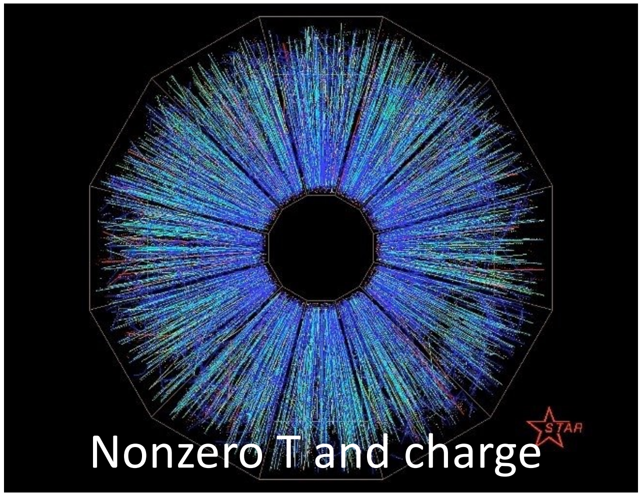

DUALITY

$\approx$

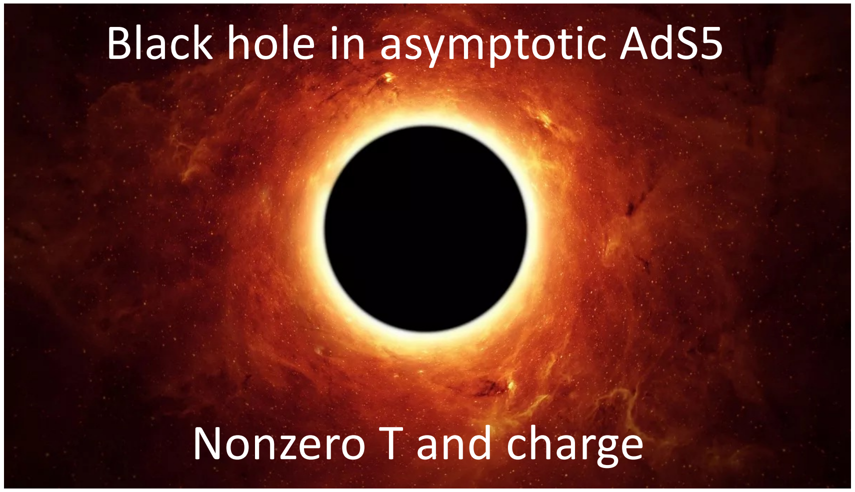

How is this used to find the QCD CP?

Black hole (brane)

Nonzero Hawking Temperature and charge

+

Anti-de Sitter (AdS) space

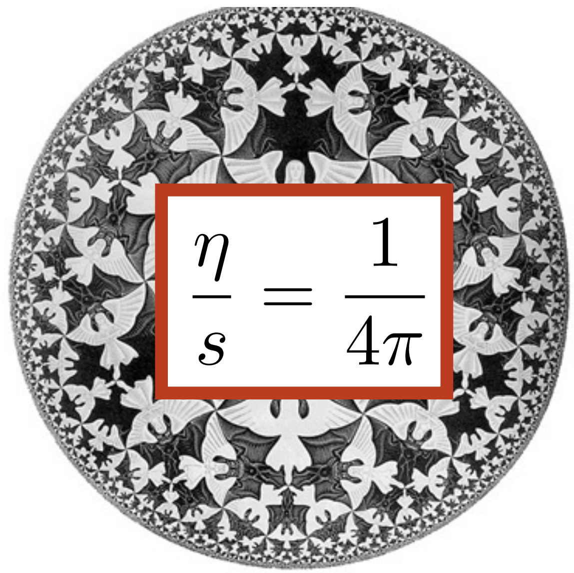

$$\frac{\eta}{s} = \frac{1}{4\pi}$$

Nearly perfect fluidity

=

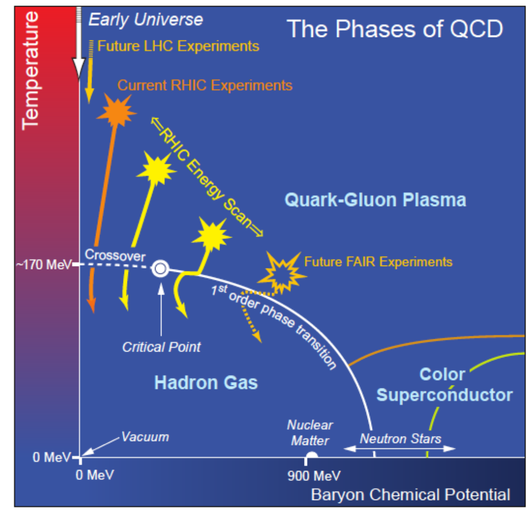

Black Hole “Engineering”

Gursoy, Kiritsis, Mazzanti, Nitti, JHEP (2008), PRL (2008)
Gubser and Nellore, PRD (2008)
DeWolfe, Gubser, Rosen, PRD (2011)
Finazzo et al, JHEP (2015)
Rougemont et al. PRL (2015), JHEP (2016),PRD (2017)
Critelli et al, PRD (2017)
Grefa et al, PRD (2021), PRD (2022)
Hippert et al, PRD (2024)

+ MANY OTHERS!!!

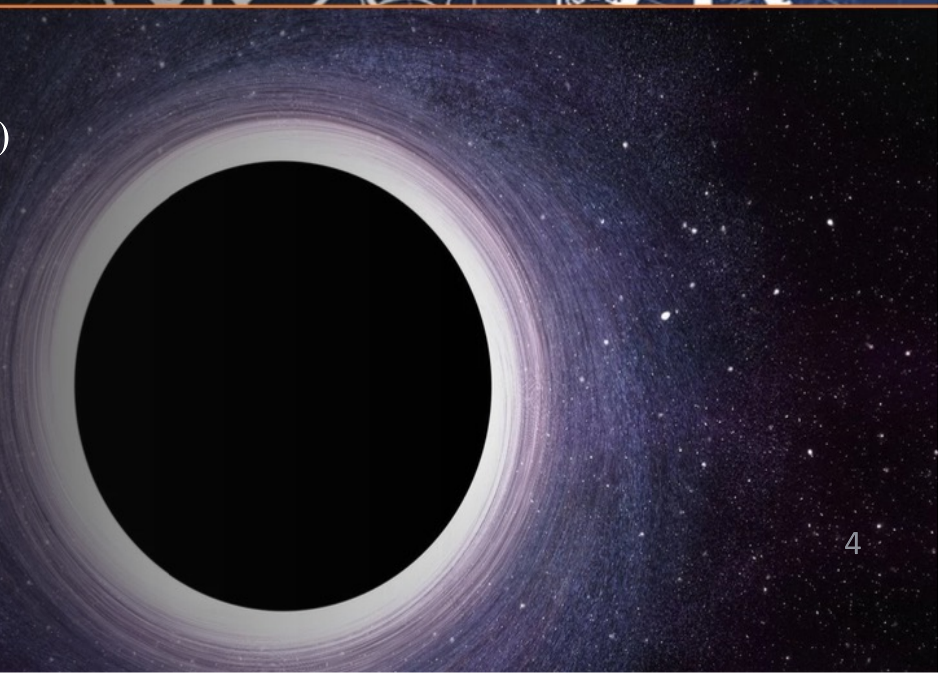

Black hole engineering in AdS

- Black hole solutions of Einstein-Maxwell-Dilaton equations

See the review by Rougemont et al, Progress in Particle and Nuclear Physics 135 (2024)

$$S = \frac{1}{2\kappa_5^2}\int_{\mathcal{M}_5} d^5x\sqrt{-g}\left[R - \frac{(\partial_\mu\phi)^2}{2} - V(\phi) - \frac{f(\phi)F_{\mu\nu}^2}{4}\right]$$

Dilaton field dual to $\langle \mathrm{Tr}F^2 \rangle$

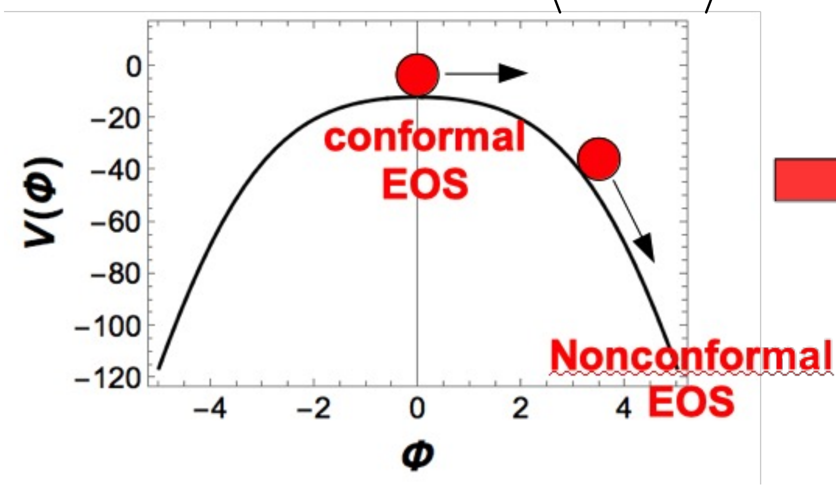

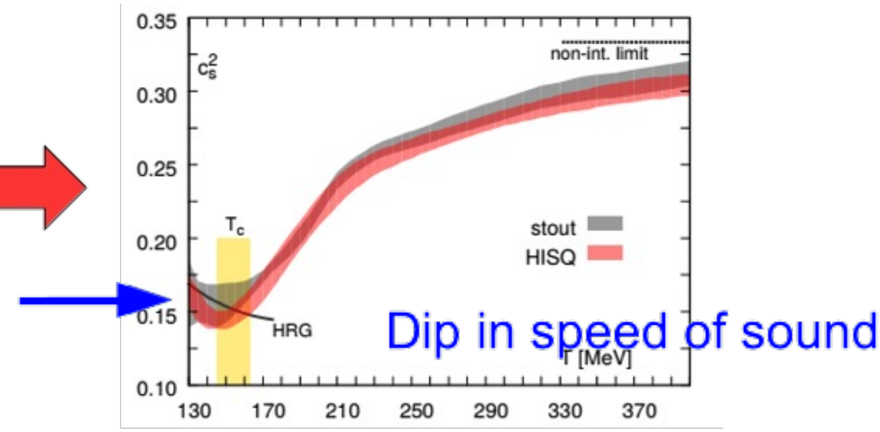

Black hole engineering in AdS

- Black hole solutions of Einstein-Maxwell-Dilaton equations

See the review by Rougemont et al, Progress in Particle and Nuclear Physics 135 (2024)

$$S = \frac{1}{2\kappa_5^2} \int_{\mathcal{M}_5} d^5x \sqrt{-g} \left[R - \frac{(\partial_\mu \phi)^2}{2} - V(\phi) - \frac{f(\phi) F_{\mu\nu}^2}{4} \right]$$

Dilaton field dual to $\langle \mathrm{Tr} F^2 \rangle$

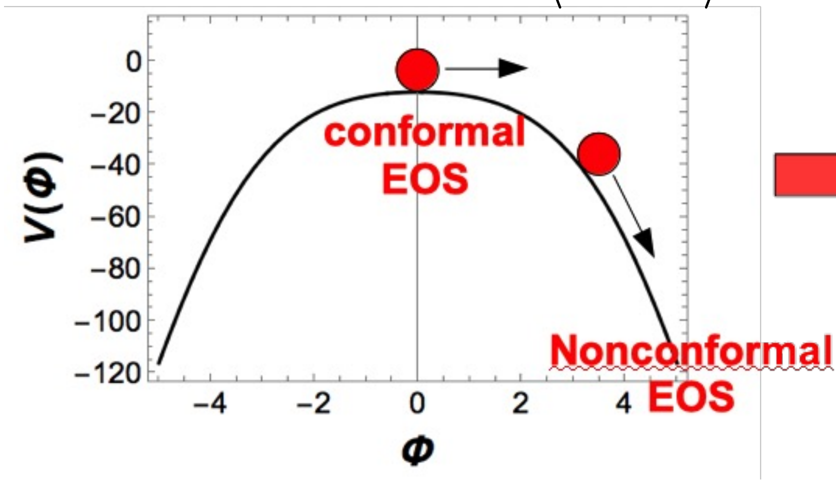

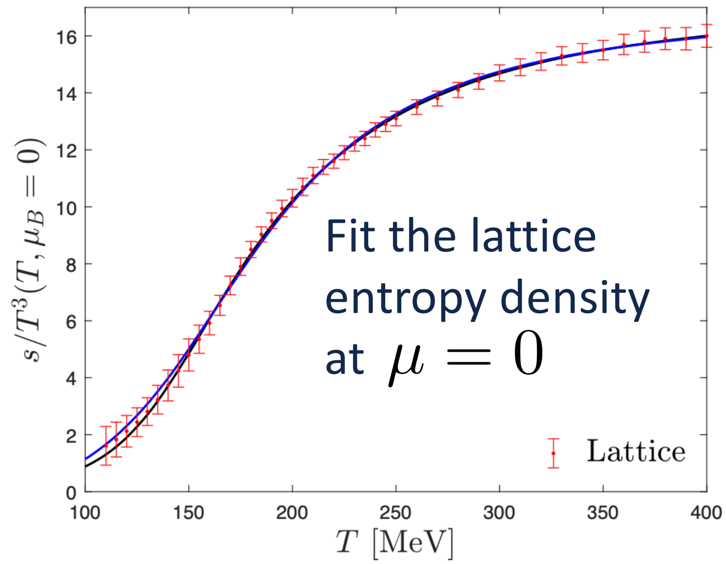

Fit the lattice entropy density at $\mu = 0$

Black hole engineering in AdS

- Black hole solutions of Einstein-Maxwell-Dilaton equations

See the review by Rougemont et al, Progress in Particle and Nuclear Physics 135 (2024)

$$S = \frac{1}{2\kappa_5^2}\int_{\mathcal{M}_5} d^5x\sqrt{-g}\left[R - \frac{(\partial_\mu\phi)^2}{2} - V(\phi) - \frac{f(\phi)F_{\mu\nu}^2}{4}\right]$$

5d gauge field | Conserved baryon charge | Dilaton-Maxwell coupling

$A_\mu \Longrightarrow U(1)_B$ $\quad f(\phi)$

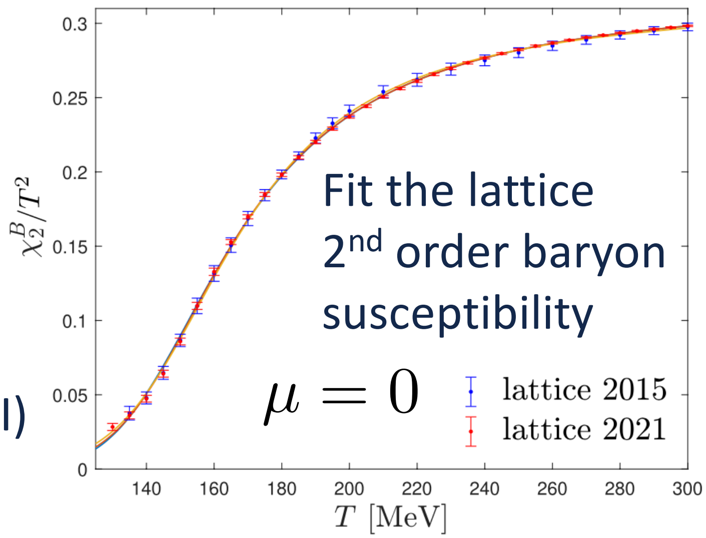

Backreaction from quark flavor branes (approx. of DBI)
(describes chirally symmetric phase)

Finite density properties

Grefa et al, Phys. Rev. D 104, 034002 (2021)
Grefa et al, Phys. Rev. D 106 (2022) 034024

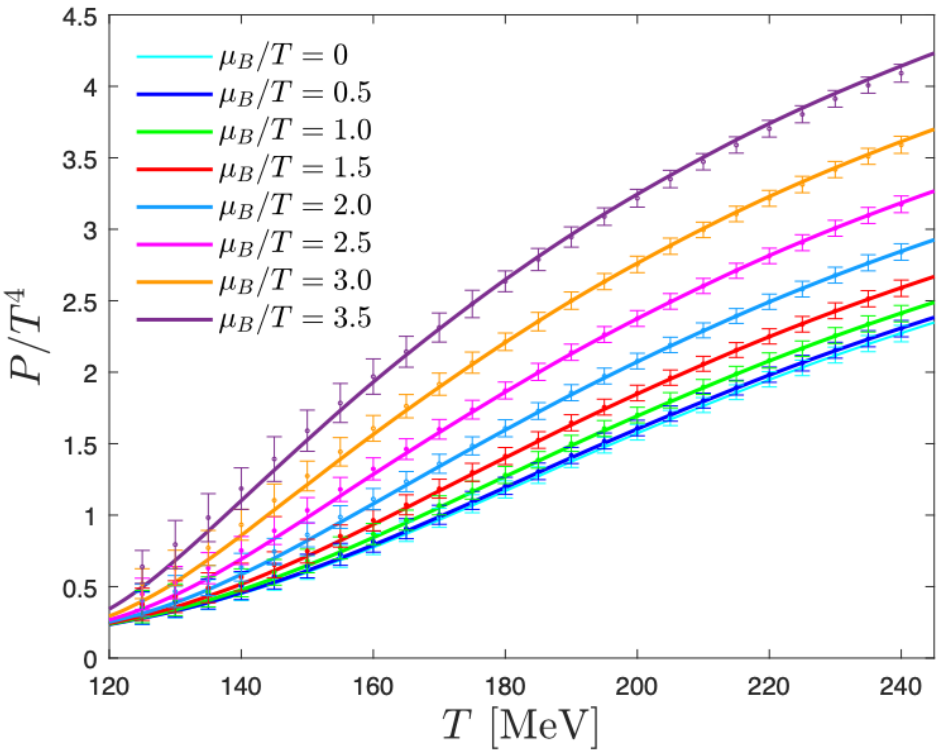

Hippert et al. PRD (2024)

Lattice: Borsányi et al, PRL 126 (2021)

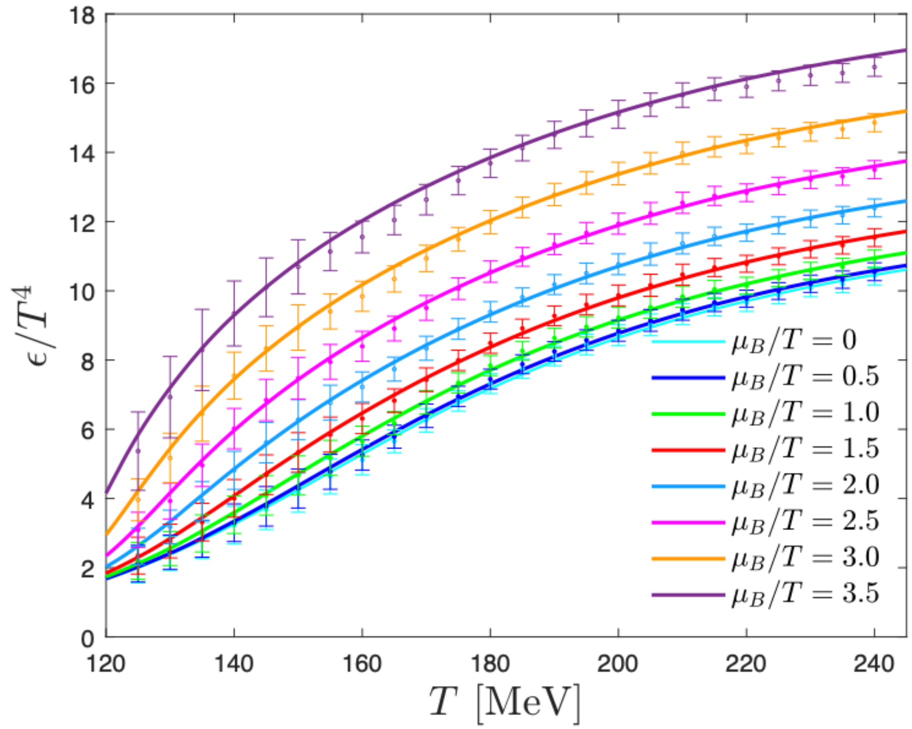

- Predictive model for baryon-rich QGP
- Real-time calculations (e.g. transport, hydro) possible

Precise determination of phase diagram

Hippert et al, PRD (2024)

- Dilaton and electric fields at horizon: ϕ_0 and Φ_1 fully specify the physical state.
- Lines of constant ϕ_0 can cross.
- Metastable states, spinodal lines.
- Critical point: where crossings start.
  Fast algorithm to find CP!
- Maxwell construction: first-order line.

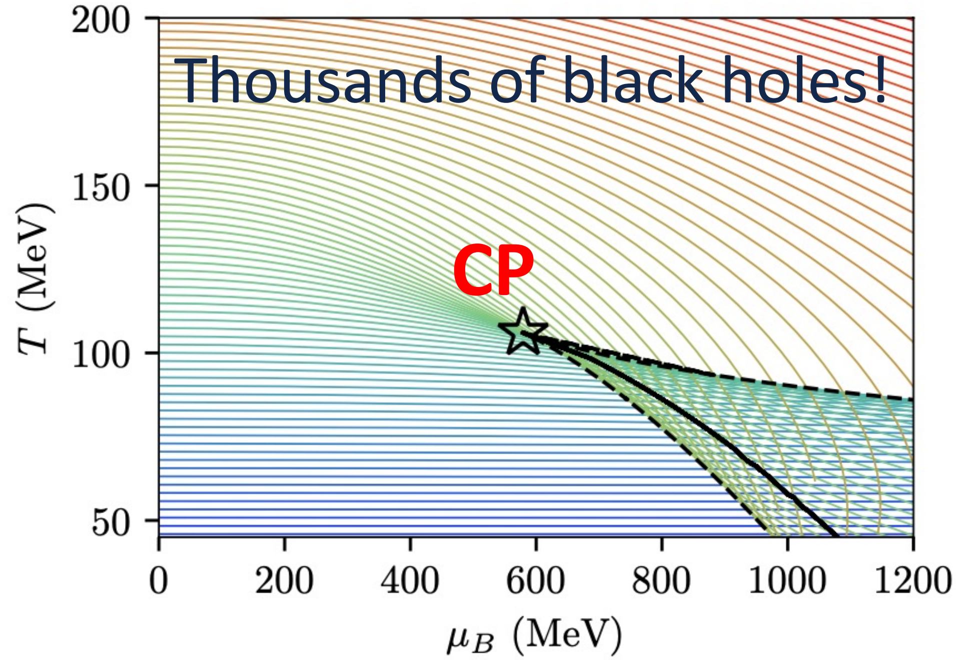

Fast and precise new algorithm = ripe for statistical analysis!

How do the many parameters affect CP?

Hippert et al, PRD (2024)

Polynomial-Hyperbolic Ansatz (PHA)

- Interpolates between Phys. Rev. D 96 (2017) and Phys. Rev. D 104 (2021)

$$V(\phi) = -12\cosh(\gamma\,\phi) + b_2\,\phi^2 + b_4\,\phi^4 + b_6\,\phi^6$$

$$f(\phi) = \frac{\operatorname{sech}(c_1\phi + c_2\phi^2 + c_3\phi^3)}{1+d_1} + \frac{d_1}{1+d_1}\operatorname{sech}(d_2\phi)$$

Parametric Ansatz (PA)

- Similar shapes, more interpretable parameters Phys. Rev. D 96 (2017)

$$V(\phi) = -12\cosh\left[\left(\frac{\gamma_1\,\Delta\phi_V^2 + \gamma_2\,\phi^2}{\Delta\phi_V^2 + \phi^2}\right)\phi\right]$$

$$f(\phi) = 1 - (1-A_1)\left[\frac{1}{2} + \frac{1}{2}\tanh\left(\frac{\phi-\phi_1}{\delta\phi_1}\right)\right] - A_1\left[\frac{1}{2} + \frac{1}{2}\tanh\left(\frac{\phi-\phi_2}{\delta\phi_2}\right)\right]$$

Bayesian black hole engineering

Hippert et al, PRD (2024)

- How do we make sense of these parameters?
- Are CPs always present in these models?
- How do lattice results affect CP location/existence?
- Bayesian inference analysis is a useful tool here.

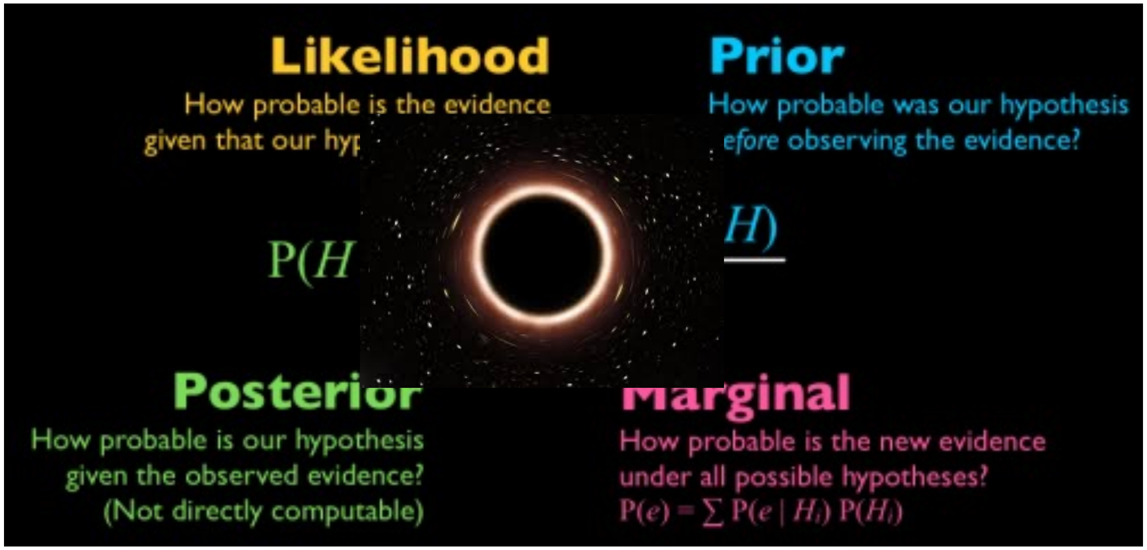

Bayesian black hole engineering

Hippert et al, PRD (2024)

Assigning probabilities

muses

Bayes' Theorem

$$\underbrace{P\left(\text{model}\,\middle|\,\text{results}\right)}_{\text{posterior } \mathcal{P}} \times P\left(\text{results}\right) = \underbrace{P\left(\text{results}\,\middle|\,\text{model}\right)}_{\text{likelihood } \mathcal{L}} \times \underbrace{P\left(\text{model}\right)}_{\text{prior knowledge}}$$

Gaussian Likelihood

$$\mathcal{L} = \exp\left\{-\frac{1}{2}\boldsymbol{\delta x}^T \boldsymbol{\Sigma}^{-1}\boldsymbol{\delta x} - \frac{1}{2}\log\det\boldsymbol{\Sigma} + \text{constant}\right\}$$

- $\boldsymbol{\delta x}$: deviation for $\boxed{s(T) \text{ and } \chi_2^{(B)}(T) \text{ at } \mu = 0.}$
- Correlation $\Gamma \equiv \exp\left(-\Delta T/\xi_T\right)$ between neighboring points $\rightarrow$ extra model parameter.

Bayesian black hole engineering

muses

Hippert et al, PRD (2024)

Markov Chain Monte-Carlo (MCMC)

- Random evolution to sample from posterior.
- Transition probabilities such that $\mathcal{P}$ is stationary limit.
- Differential evolution MCMC: suited for correlations.

C.J.F. Ter Braak, Statistics and Computing **16** (2006)

Differential evolution

1. Use other chains j, k to update chain $i \neq j \neq k$: $\theta_i \to \theta_i + \frac{b}{\sqrt{2d}}(\theta_j - \theta_k) + \xi_i$.
2. Compute $\mathcal{P}$ from model EoS.
   - If $\mathcal{P}/\mathcal{P}_0 > 1$, transition to new parameters.
   - Otherwise, accept transition with probability $\mathcal{P}/\mathcal{P}_0$.
3. Repeat.

Inputs: Baryon susceptibility and entropy density from the lattice.

S. Borsanyi, Z. Fodor, C. Hoelbling, S. D. Katz, S. Krieg and K. K. Szabo, PRL **730** (2014)
Borsányi, Fodor, Guenther et al., PRL **126** (2021)

Bayesian black hole engineering

Hippert et al, PRD (2024)

- **Flat prior for parameters**
- **20% of prior samples give no CP**

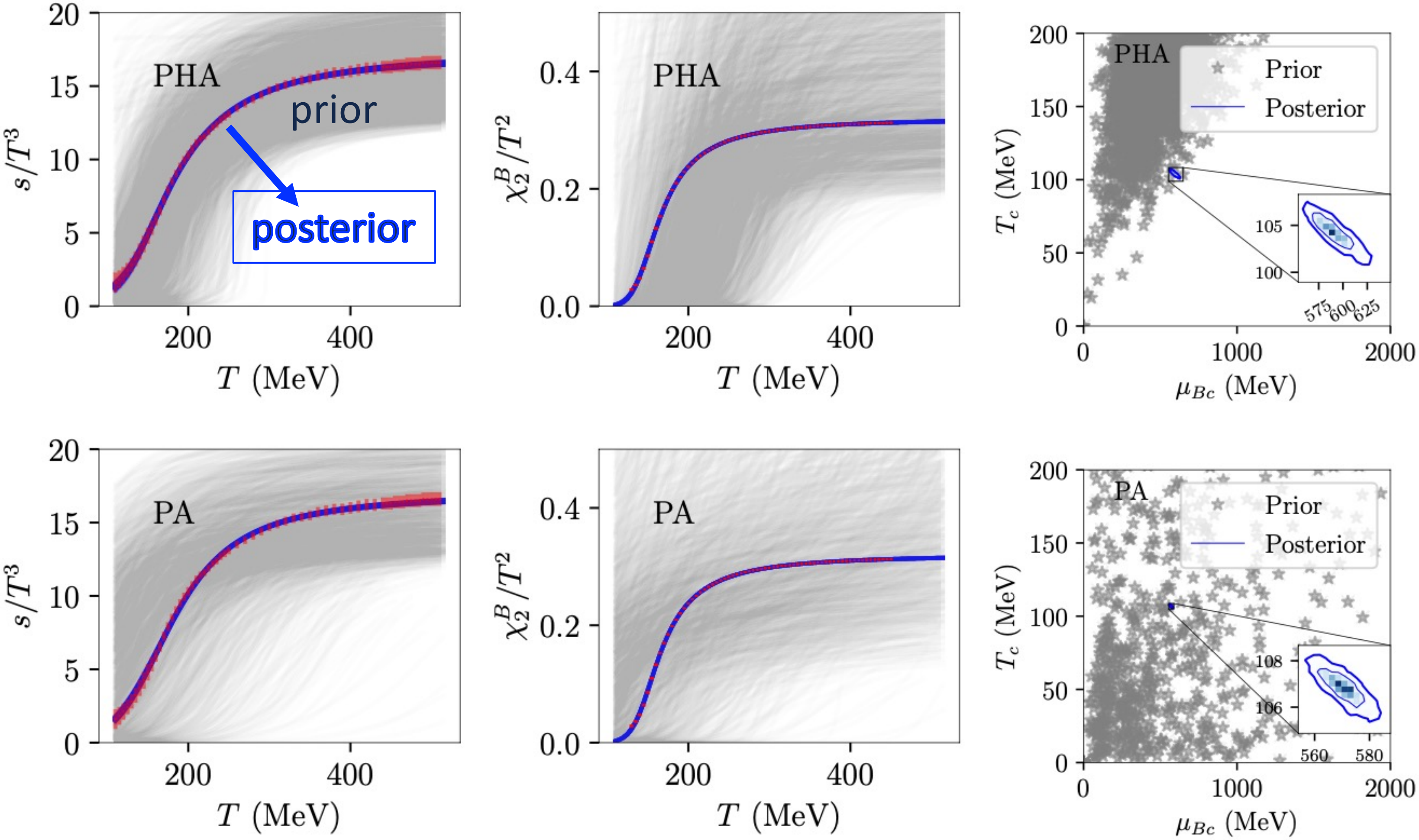

Bayesian black hole engineering

Hippert et al, PRD (2024)

All posterior predictions for CP location collapse around these regions

Posterior critical points

$(T_c,\, \mu_{Bc})_{PHA} = (104 \pm 3,\, 589^{+36}_{-26})$ MeV, $(T_c,\, \mu_{Bc})_{PA} = (107 \pm 1,\, 571 \pm 11)$ MeV.

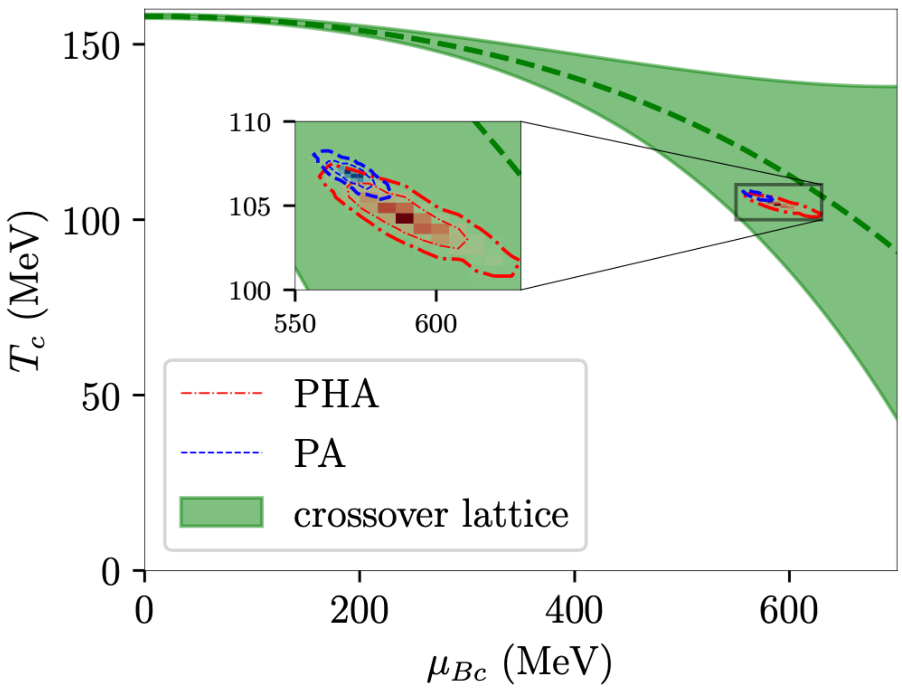

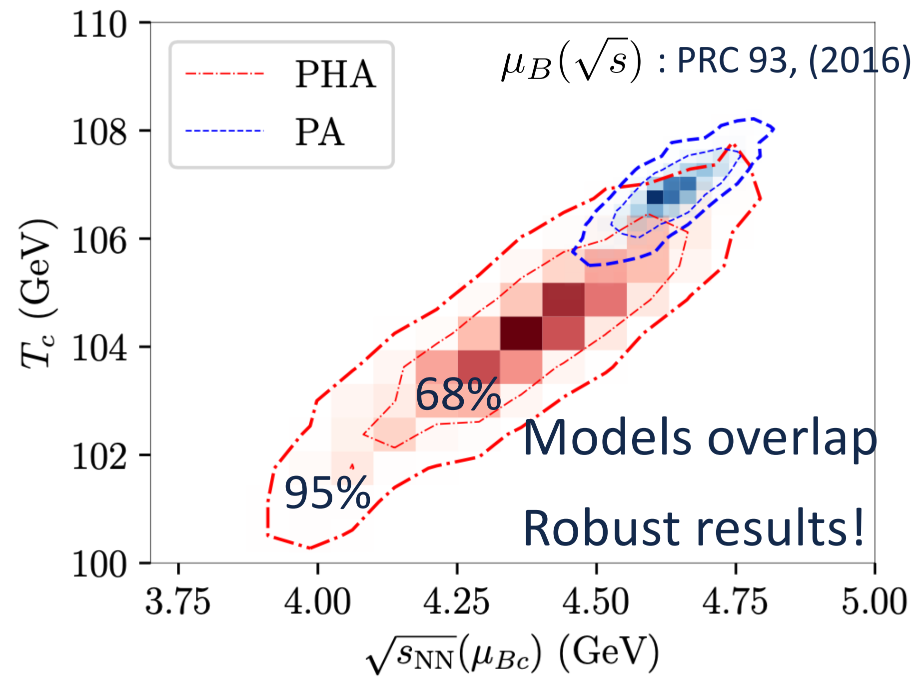

Location of CP from holography

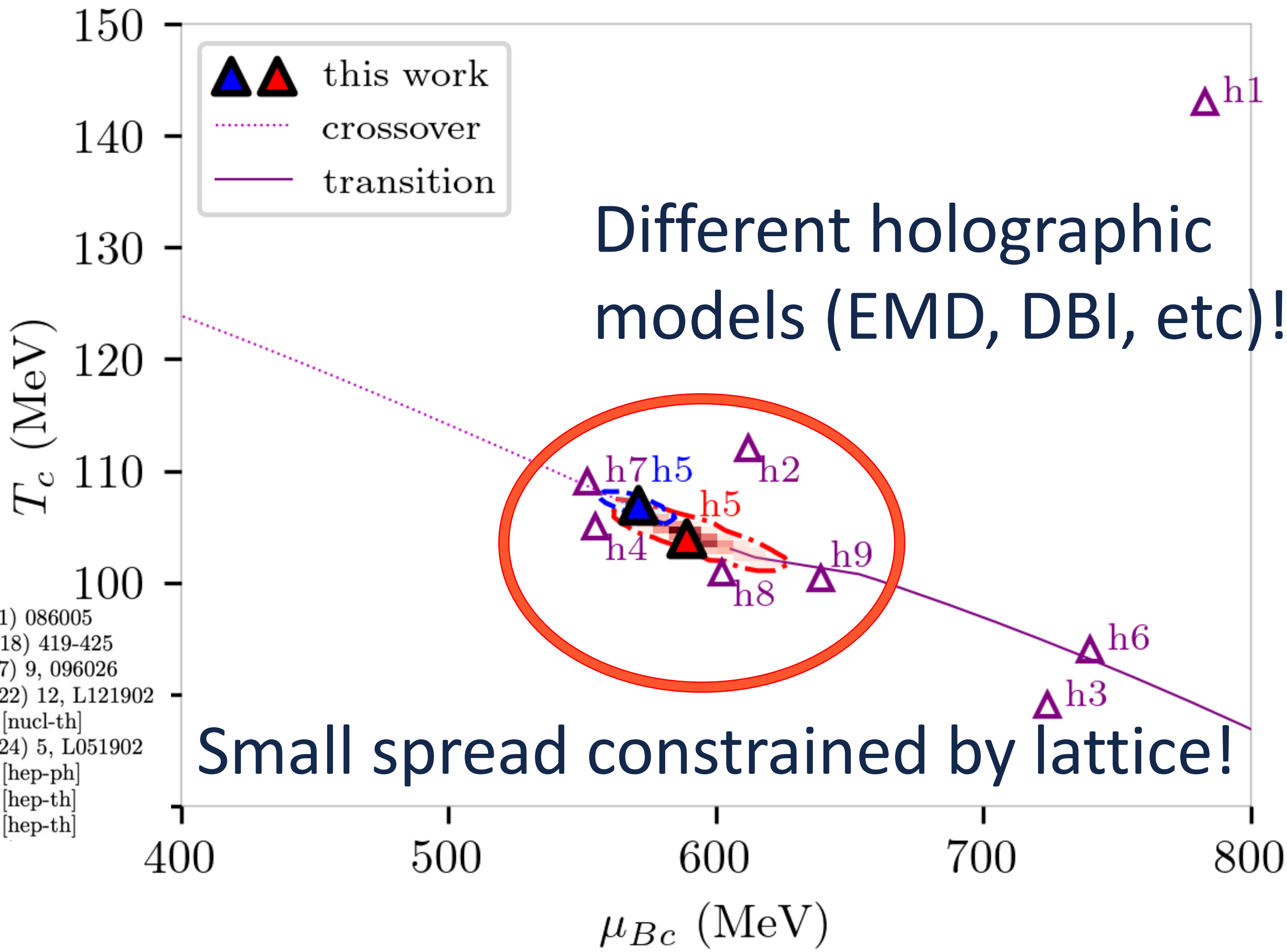

Different holographic models (EMD, DBI, etc)!

Small spread constrained by lattice!

h1: Phys.Rev.D 83 (2011) 086005
h2: Phys.Lett.B 778 (2018) 419-425
h3: Phys.Rev.D 96 (2017) 9, 096026
h4: Phys.Rev.D 106 (2022) 12, L121902
h5: e-Print: 2309.00579 [nucl-th]
h6: Phys.Rev.D 109 (2024) 5, L051902
h7: e-Print: 2404.12109 [hep-ph]
h8: e-Print: 2405.02394 [hep-th]
h9: e-Print: 2405.02394 [hep-th]

Location of CP from holography

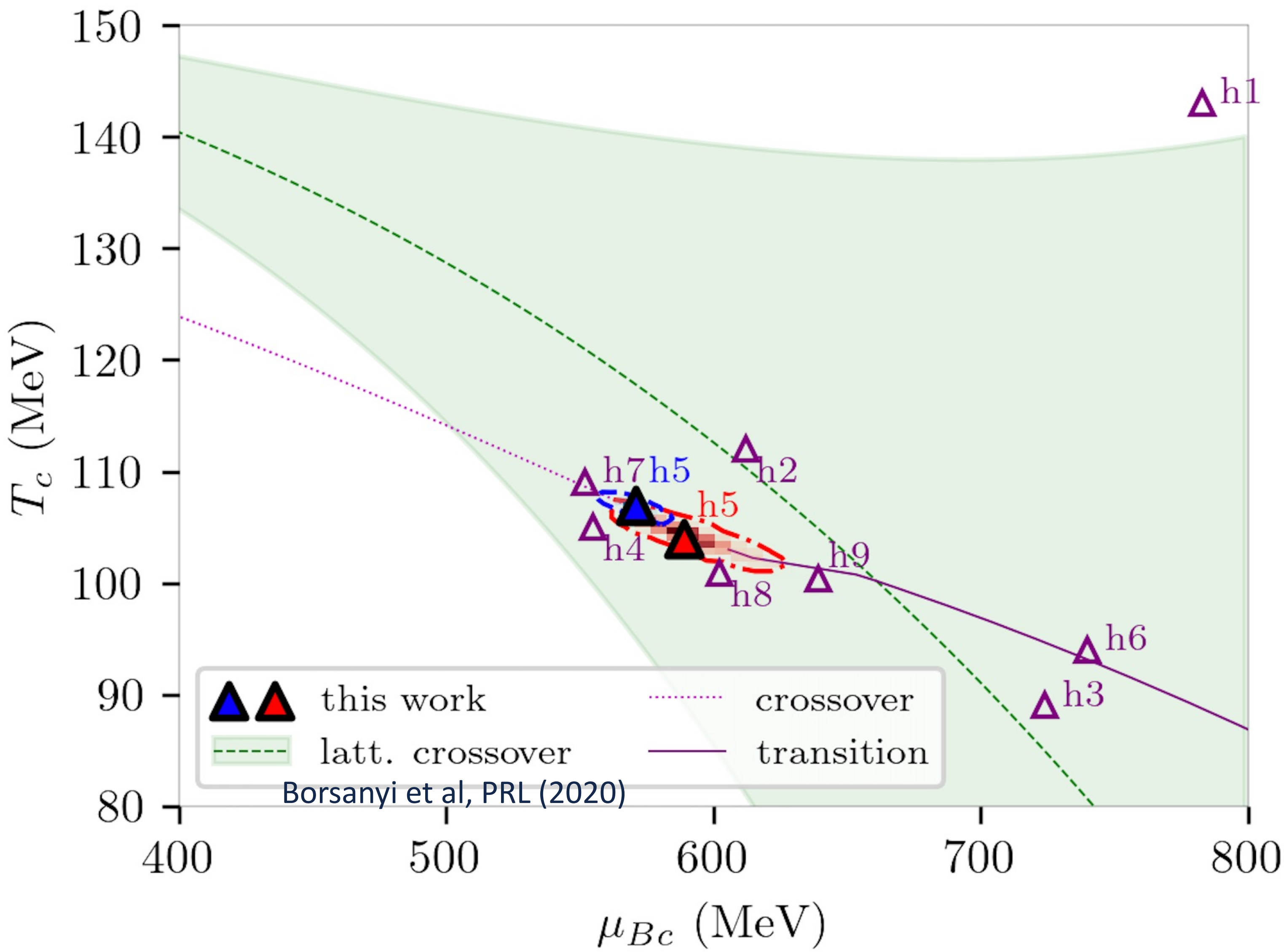

Location of CP from models: 18 years ago

M. Stephanov, Lattice 2006 Plenary talk, arXiv:hep-lat/0701002

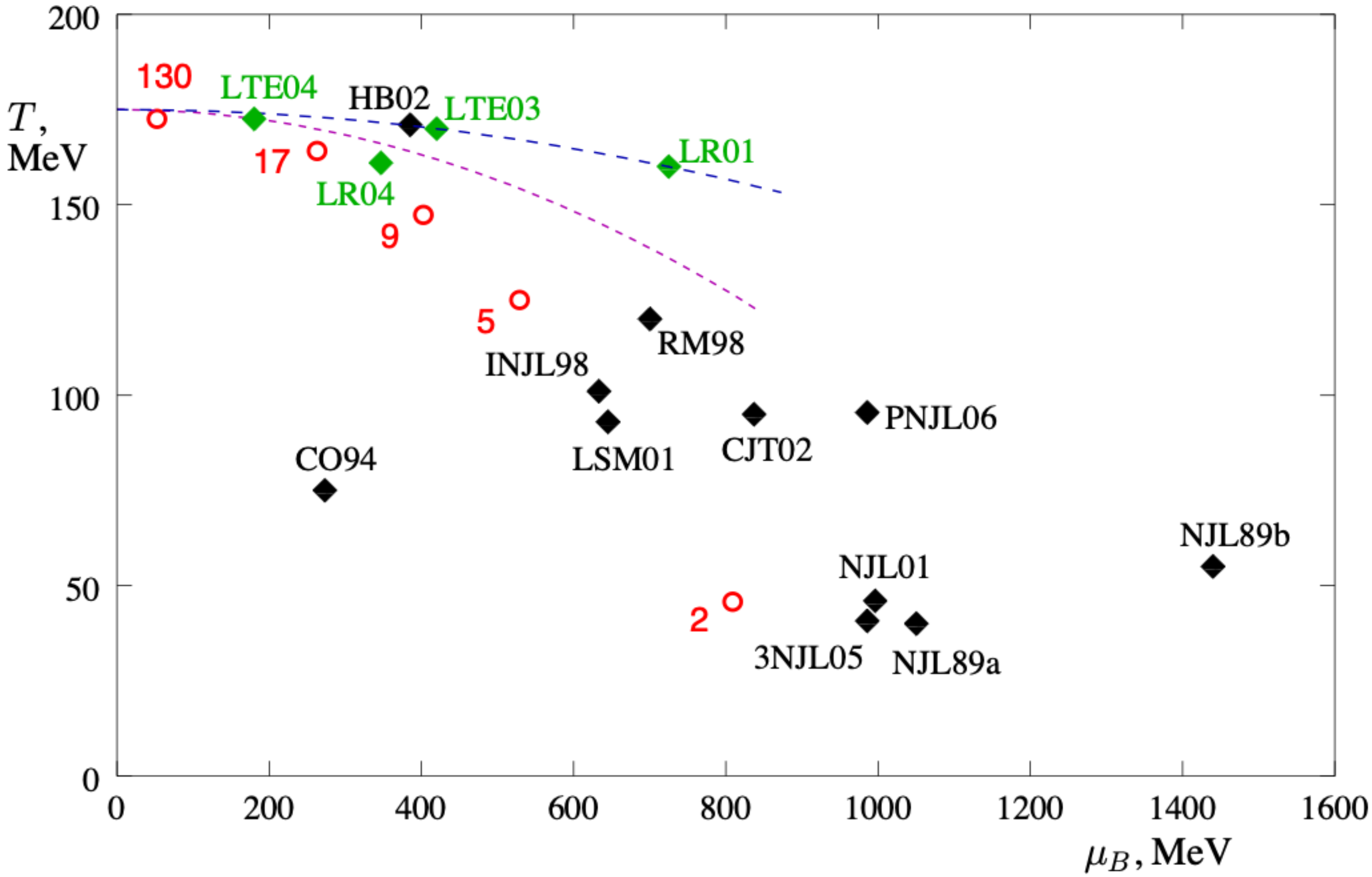

Location of CP from models: 18 years ago

M. Stephanov, Lattice 2006 Plenary talk, arXiv:hep-lat/0701002

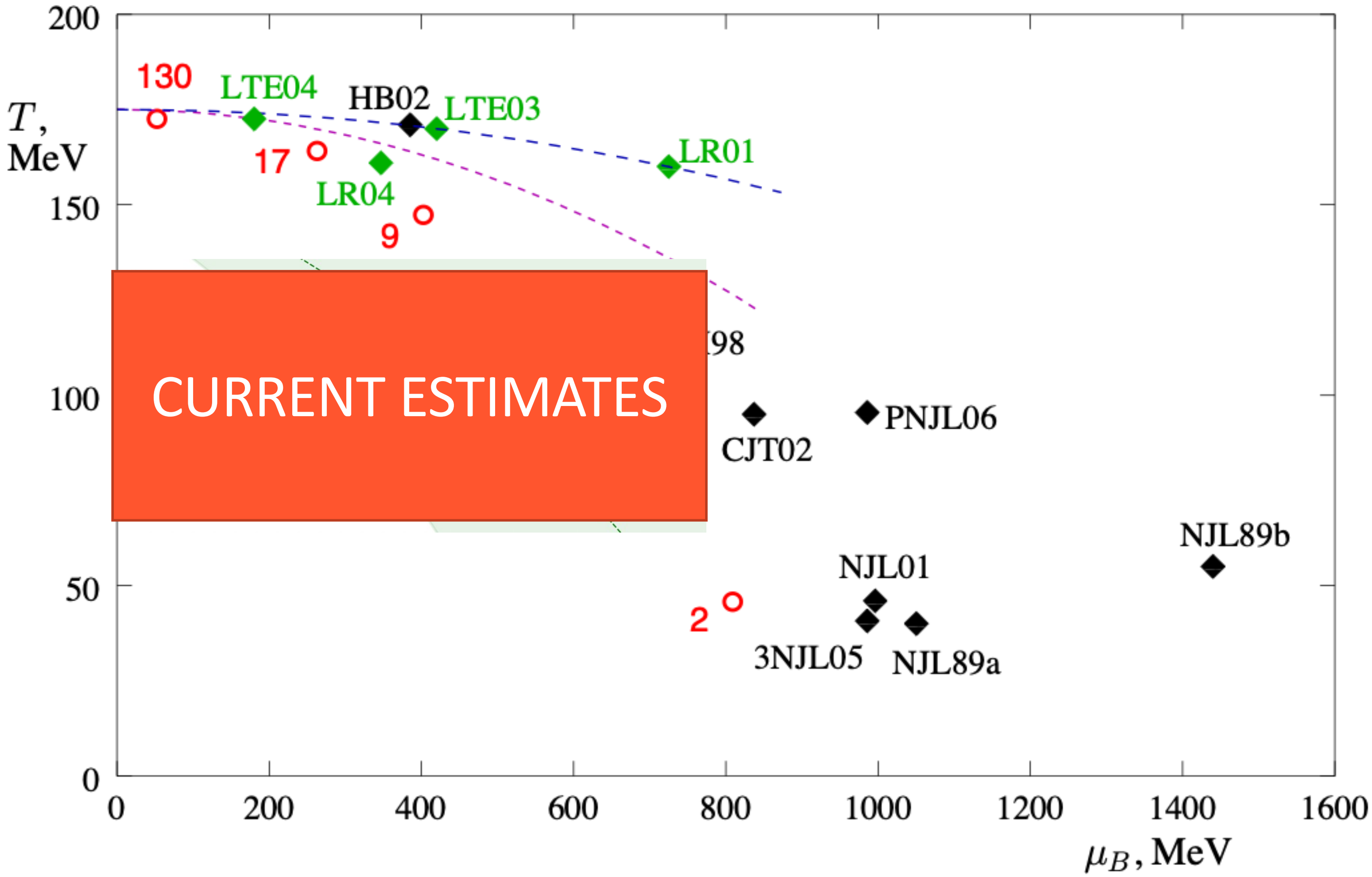

Location of CP from models: 18 years ago

M. Stephanov, Lattice 2006 Plenary talk, arXiv:hep-lat/0701002

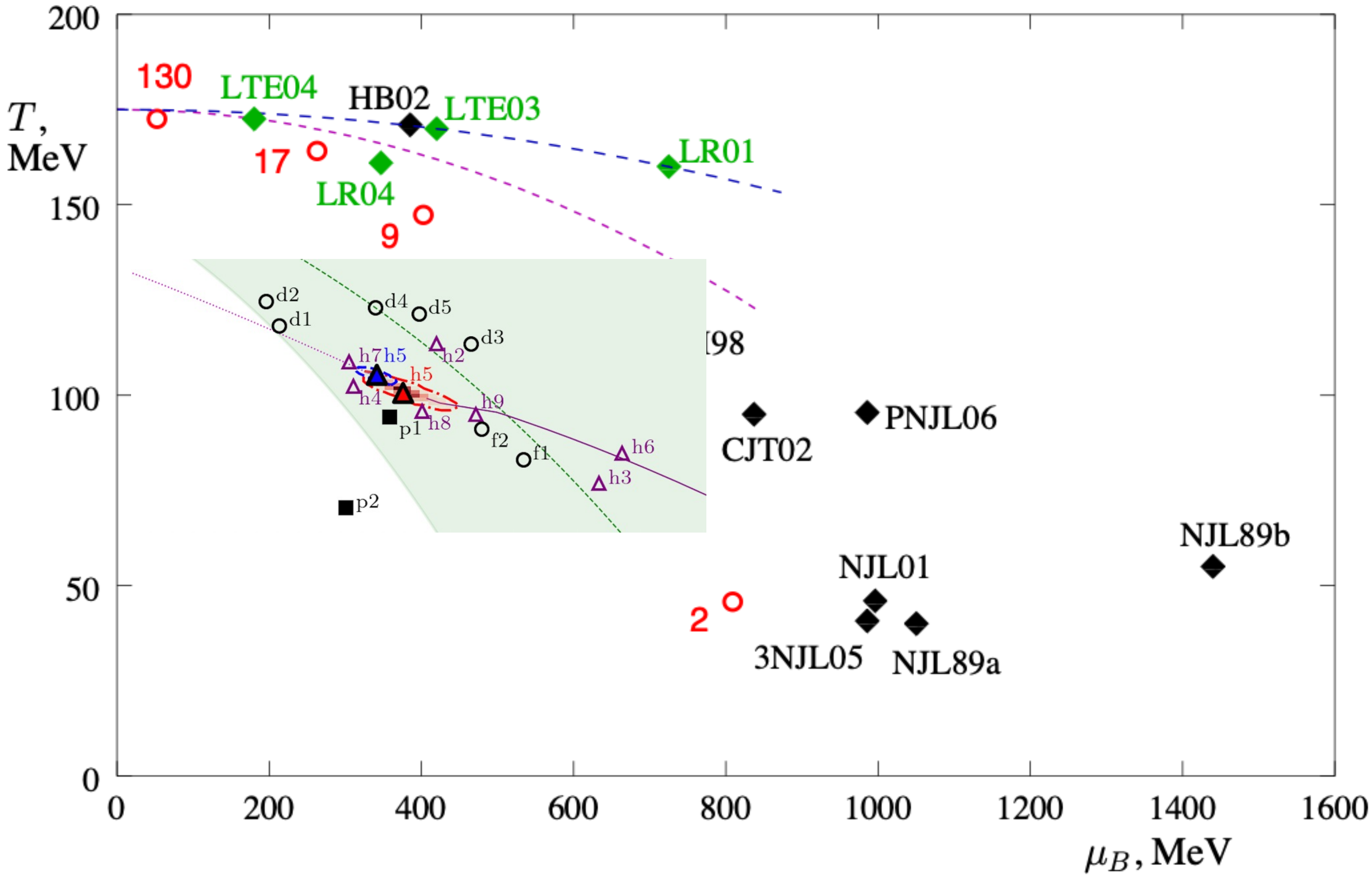

Current estimates for the CP location

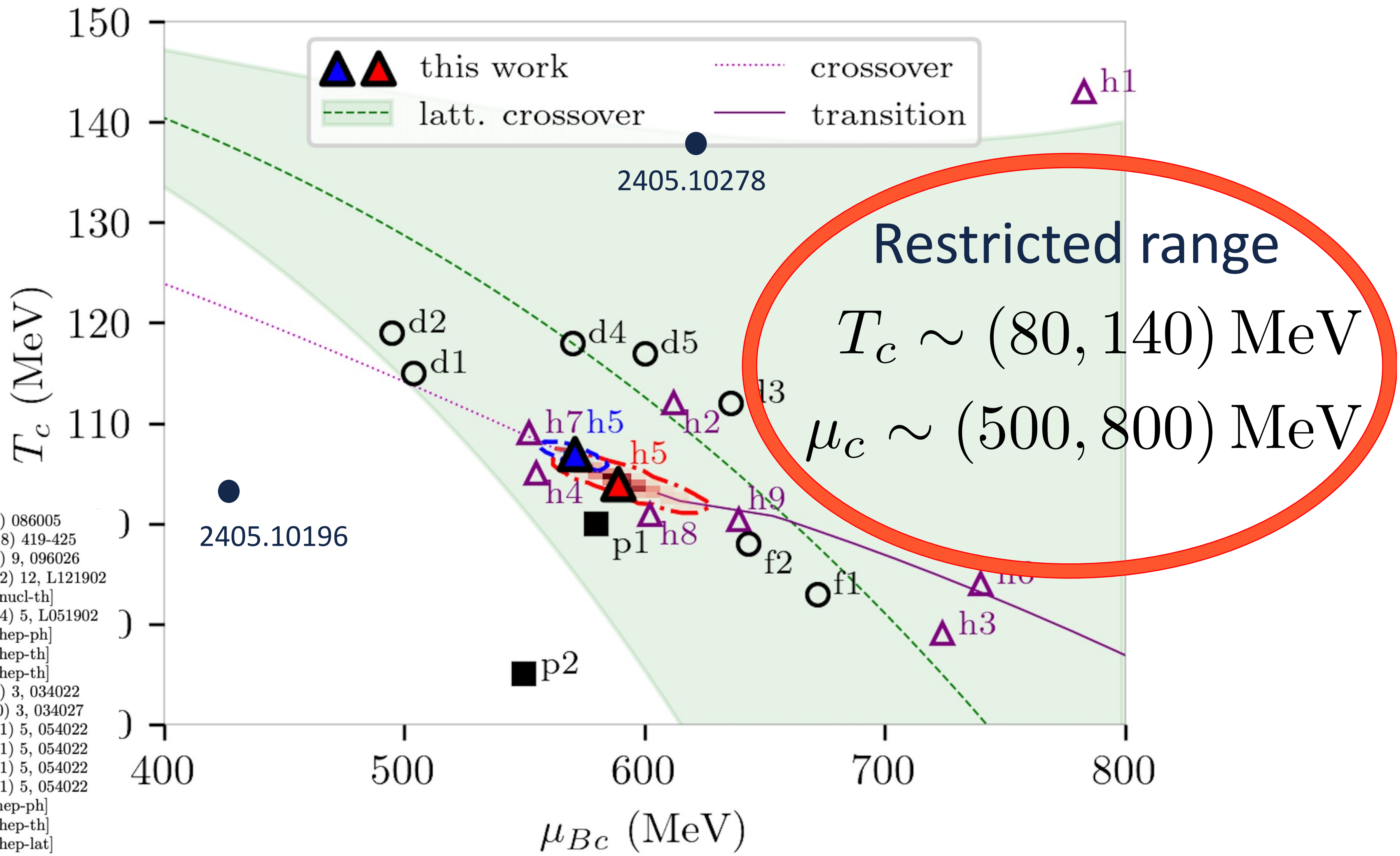

h1: Phys.Rev.D 83 (2011) 086005
h2: Phys.Lett.B 778 (2018) 419-425
h3: Phys.Rev.D 96 (2017) 9, 096026
h4: Phys.Rev.D 106 (2022) 12, L121902
h5: e-Print: 2309.00579 [nucl-th]
h6: Phys.Rev.D 109 (2024) 5, L051902
h7: e-Print: 2404.12109 [hep-ph]
h8: e-Print: 2405.02394 [hep-th]
h9: e-Print: 2405.02394 [hep-th]
d1: Phys.Rev.D 90 (2014) 3, 034022
f1: Phys.Rev.D 102 (2020) 3, 034027
d2: Phys.Rev.D 104 (2021) 5, 054022
d3: Phys.Rev.D 104 (2021) 5, 054022
d4: Phys.Rev.D 104 (2021) 5, 054022
d5: Phys.Rev.D 104 (2021) 5, 054022
f2: e-Print: 2308.15508 [hep-ph]
p1: e-Print: 2312.06952 [hep-th]
p2: e-Print: 2401.08820 [hep-lat]

Current estimates for the CP location

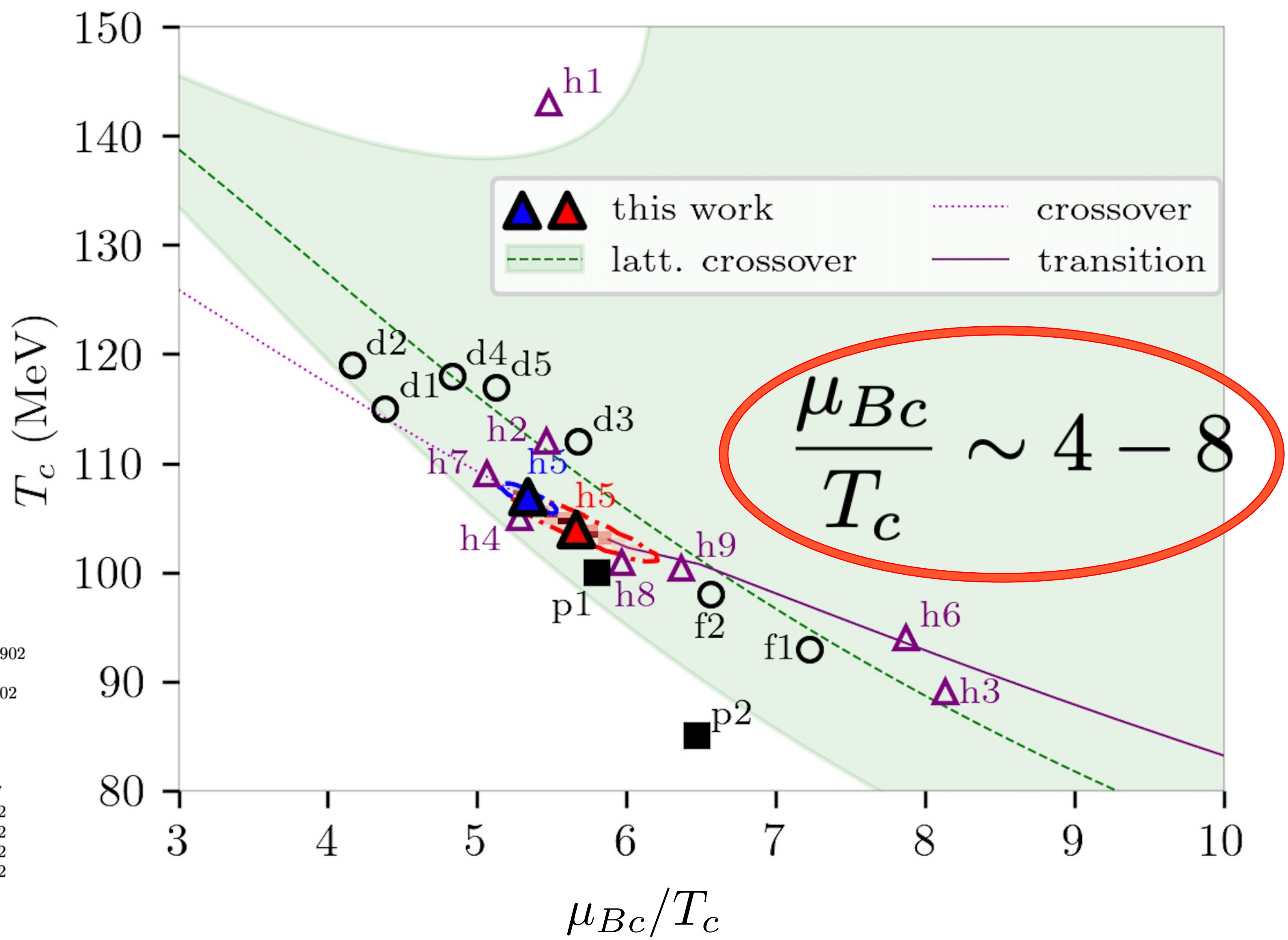

h1: Phys.Rev.D 83 (2011) 086005
h2: Phys.Lett.B 778 (2018) 419-425
h3: Phys.Rev.D 96 (2017) 9, 096026
h4: Phys.Rev.D 106 (2022) 12, L121902
h5: e-Print: 2309.00579 [nucl-th]
h6: Phys.Rev.D 109 (2024) 5, L051902
h7: e-Print: 2404.12109 [hep-ph]
h8: e-Print: 2405.02394 [hep-th]
h9: e-Print: 2405.02394 [hep-th]
d1: Phys.Rev.D 90 (2014) 3, 034022
f1: Phys.Rev.D 102 (2020) 3, 034027
d2: Phys.Rev.D 104 (2021) 5, 054022
d3: Phys.Rev.D 104 (2021) 5, 054022
d4: Phys.Rev.D 104 (2021) 5, 054022
d5: Phys.Rev.D 104 (2021) 5, 054022
f2: e-Print: 2308.15508 [hep-ph]
p1: e-Print: 2312.06952 [hep-th]
p2: e-Print: 2401.08820 [hep-lat]

Conclusions

- First Bayesian inference analysis of CP location constrained by lattice results at zero net baryon density:

Predict CEP (95% confidence level):

$$T_c = 101 - 108 \text{ MeV}$$
$$\mu_c = 560 - 625 \text{ MeV}$$

$$\frac{\mu_c}{T_c} \sim 5 - 6$$

- Other approaches (FRG,DSE, FSS, Pade, etc) predict CP in a similar narrow range.

- They didn't have to agree, but they do: *who ordered that?*

EXTRA SLIDES

High-order baryon susceptibilities

Critelli et al, PRD (2017)

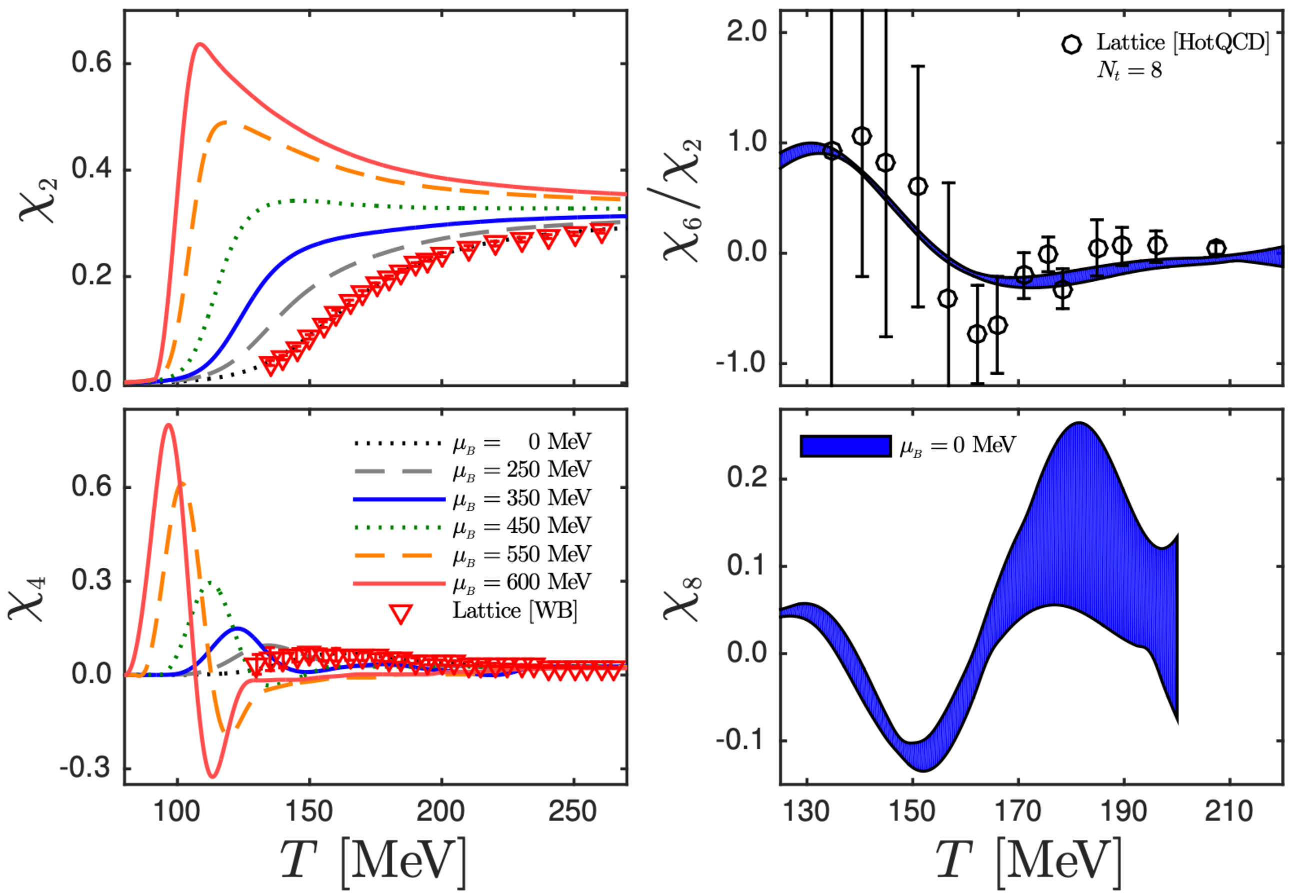

- Prediction for chi8 in 2017 compatible with lattice results (though not continuum extrapolated by then).

Critelli et al, PRD (2017)

Lattice: Borsányi et al, JHEP (2018)

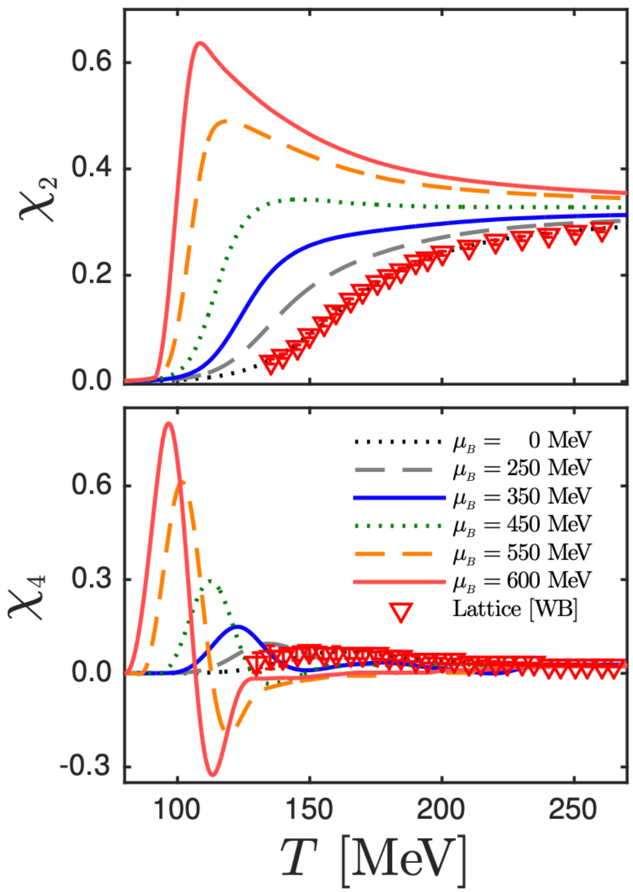

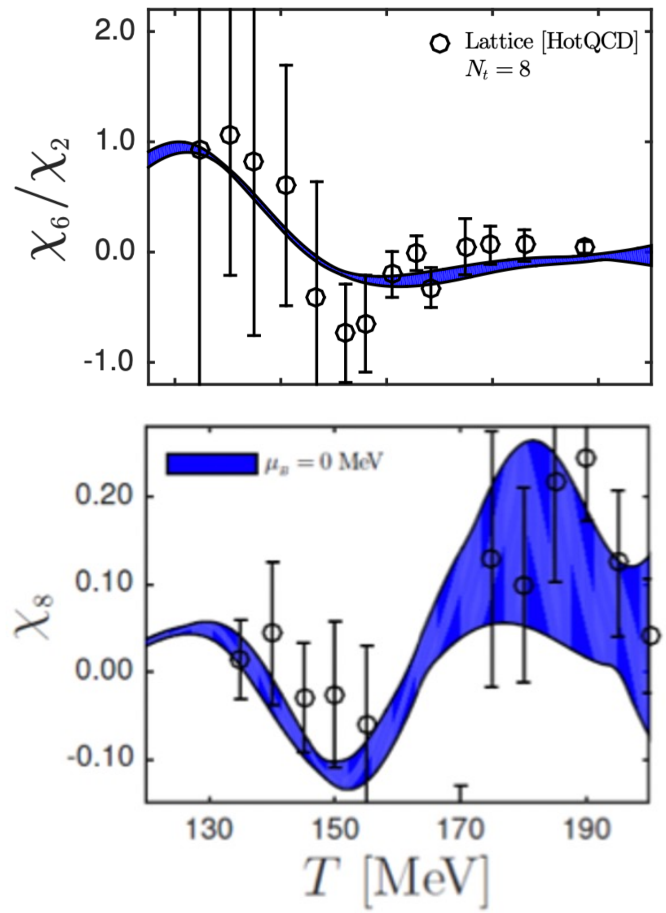

Ratio between baryon susceptibilities

Critelli et al, PRD (2017)

The shape and monotonicity properties depend on the path in the phase diagram: seeing a peak is important!

Mroczek et al, PRC (2021)

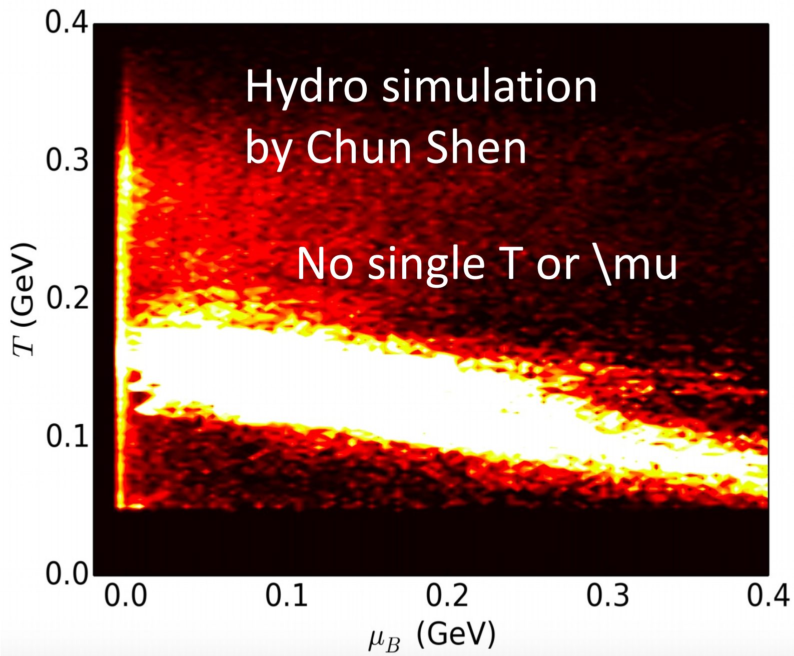

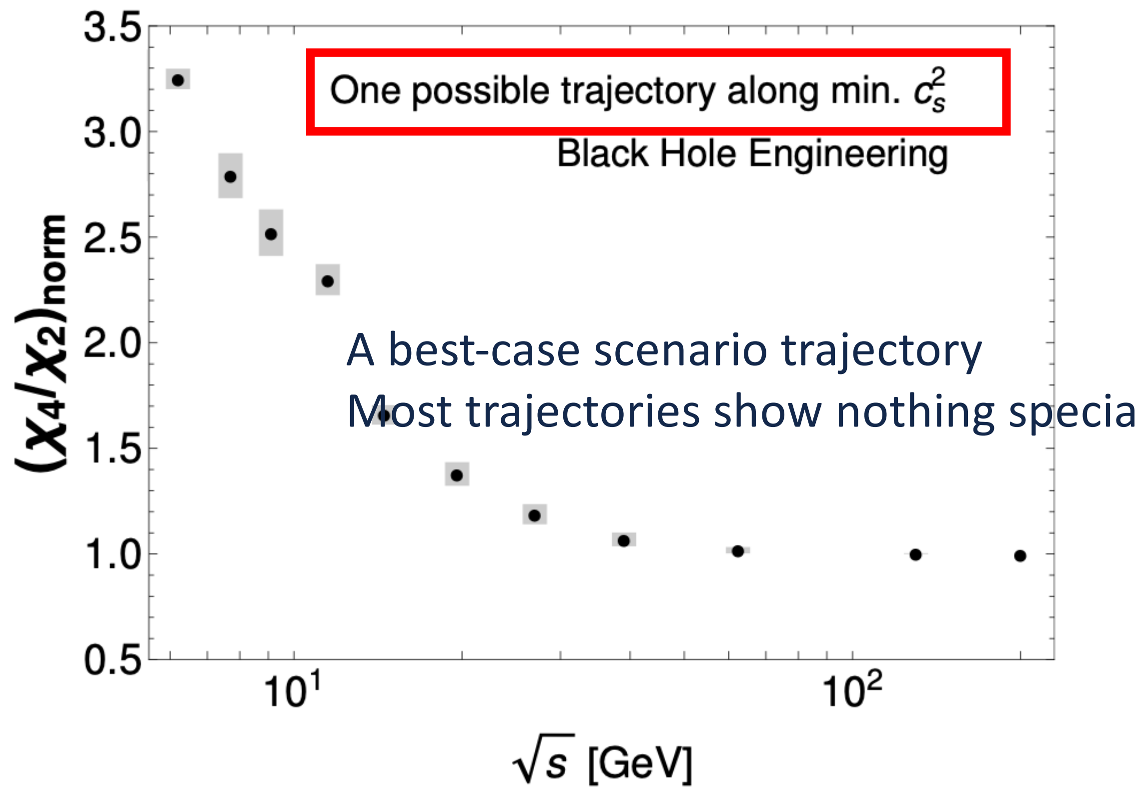

Ratio between baryon susceptibilities

Critelli et al, PRD (2017)

The shape and monotonicity properties depend on the path in the phase diagram: seeing a peak is important!

Mroczek et al, PRC (2021)

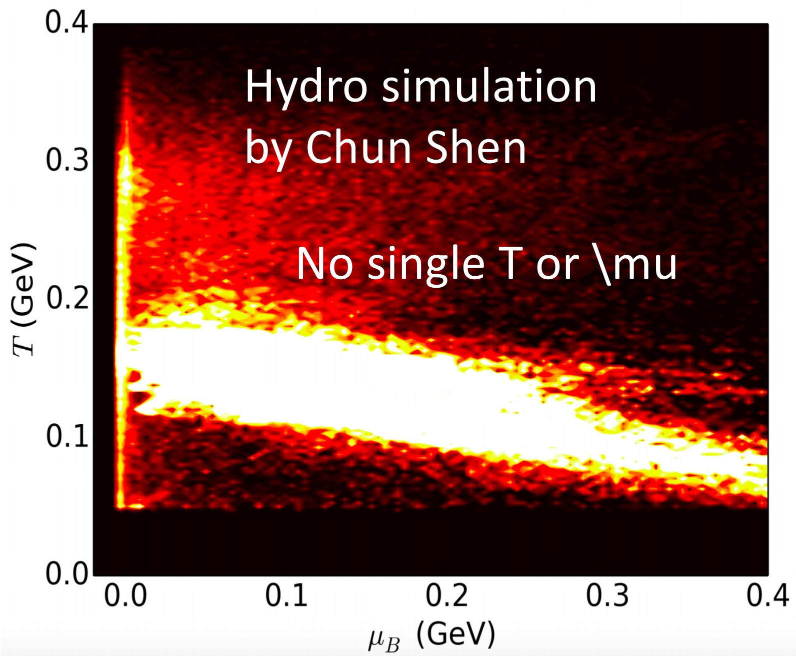

From
Jokela, Jarvinen, and Piispa, 2405.02394v1 [hep-th]

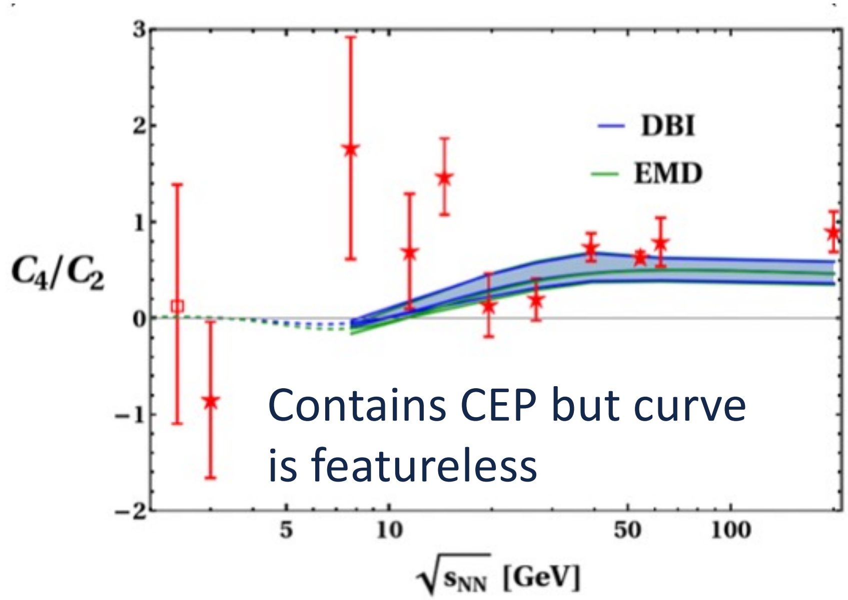

Prior distributions

FLAT PRIOR

e-Print: 2309.00579 [nucl-th]

PHA Ansatz		
Parameter	min	max
Λ	800 MeV	1400 MeV
κ_2	9.0	15.0
γ	0.5682	0.6500
b_2	-0.05	0.65
b_4	-0.150	-0.015
b_6	-0.00200	0.00169
c_1	-0.035	0.100
c_2	0.1	1.5
c_3	0.0	1.0
d_1	0.0	2.5
d_2 (J)	3	10000

PA Ansatz		
Parameter	min	max
Λ	400 MeV	1400 MeV
κ_2	9.0	15.0
γ_1	0.40	0.57
γ_2	0.50	0.68
$\Delta\phi_V$	1.5	3.0
A	0.25	0.50
ϕ_1	-0.1	0.5
$\delta\phi_1$ (J)	10^{-5}	0.3
ϕ_2	0.8	4.5
$\delta\phi_2$	0.2	4.0

TABLE I. Prior ranges for parameters in the PHA (left) and PA (right) models. The '(J)' marks parameters for which we have used *Jeffreys* priors — i.e., prior distributions that are uniform over the logarithm of these parameters.

Posterior distributions

e-Print: 2309.00579 [nucl-th]

PHA	Posterior 95% CI		
Parameter	min	max	MAP
Λ	1089 MeV	1190 MeV	1129 MeV
κ_2	11.3	11.5	11.4
γ	0.57	0.63	0.58
b_2	0.1	0.5	0.2
b_4	-0.06	-0.03	-0.05
b_6	0.000	0.002	0.0007
c_1	-0.1	0.1	0.0
c_2	0.1	0.3	0.2
c_3	0.01	0.08	0.04
d_1	1.70	1.74	1.72
d_2 (J)	113	8068	1294

PA	Posterior 95% CI		
Parameter	min	max	MAP
Λ	862 MeV	1043 MeV	955 MeV
κ_2	11.3	11.5	11.4
γ_1	0.50	0.54	0.52
γ_2	0.60	0.62	0.61
$\Delta\phi_V$	1.6	2.1	1.8
A	0.369	0.374	0.371
ϕ_1	0.000	0.025	0.002
$\delta\phi_1$ (J)	0.0001	0.0032	0.0003
ϕ_2	2.1	2.3	2.2
$\delta\phi_2$	0.65	0.73	0.69

TABLE II. Posterior 95% confidence intervals (95% CI) and maximum a posteriori (MAP) values for parameters of the PHA (left) and PA (right) models. The '(J)' marks parameters for which we have used *Jeffreys* priors — i.e., prior distributions that are uniform over the logarithm of these parameters. MAP values are extracted by maximizing the likelihood.

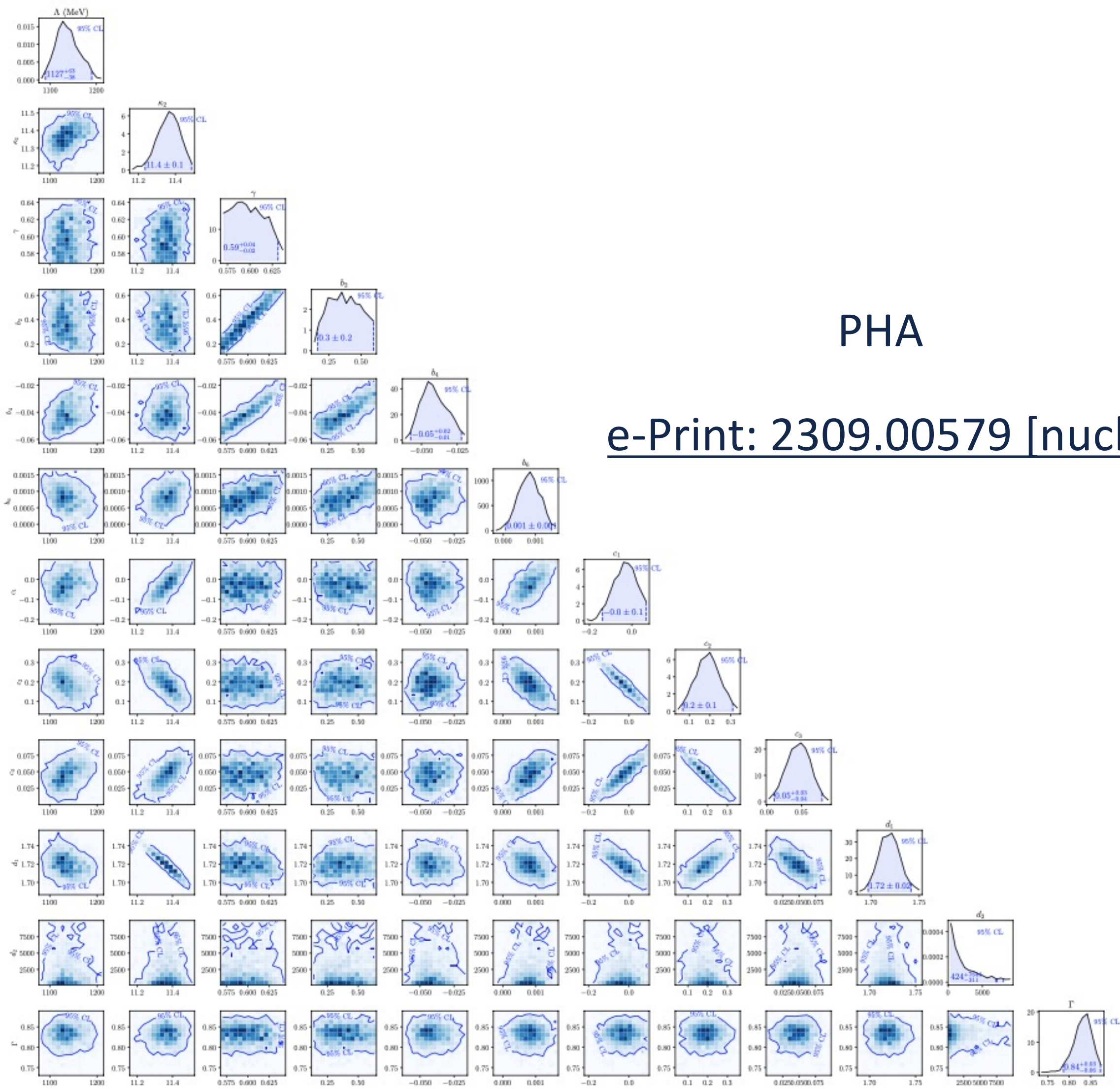

FIG. 5. Marginalized a posteriori probability distributions for pairs of parameters of the PHA model. Solid lines show 95% confidence intervals. On the diagonal, marginalized one-parameter posterior distributions are also shown, along with the marginalized maximum a posteriori (MMAP) value and 95% confidence interval for each parameter. MMAP values are extracted by maximizing the marginalized one-parameter posterior distributions.

PHA

e-Print: 2309.00579 [nucl-th]

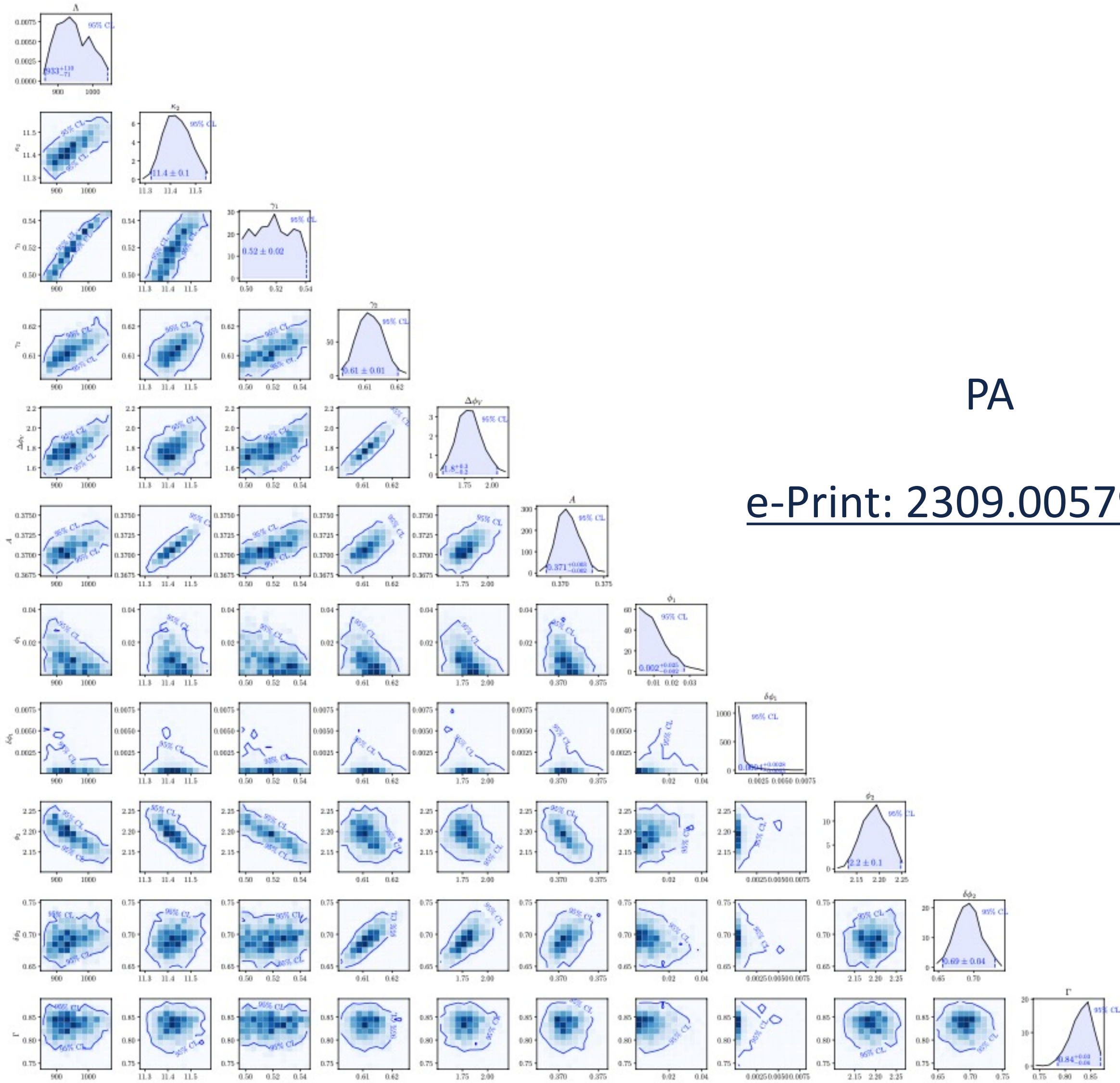

FIG. 6. Marginalized a posteriori probability distributions for pairs of parameters of the PA model. Solid lines show 95% confidence intervals. On the diagonal, marginalized one-parameter posterior distributions are also shown, along with the marginalized maximum a posteriori (MMAP) value and 95% confidence interval for each parameter. MMAP values are extracted by maximizing the marginalized one-parameter posterior distributions.

PA

e-Print: 2309.00579 [nucl-th]

e-Print: 2309.00579 [nucl-th]

LIKELIHOOD FUNCTION

The agreement between predictions $\vec{p}(\theta)$ of the model with parameters θ and lattice QCD results $\vec{d}$ is quantified by the likelihood function $\mathcal{L}(\vec{\theta}) \equiv P(\vec{d}|\vec{\theta})$.

We take a Gaussian likelihood

$$\mathcal{L}(\vec{\theta}) = \frac{1}{\prod\limits_{Q=s,\chi_2} \left[\left(\prod\limits_i \sigma_i^{(Q)} \right) \sqrt{2\pi \det \Lambda} \right]} \exp\left\{ -\frac{1}{2} \sum_{i,j} \sum_{Q=s,\chi_2} \frac{p_i^{(Q)}(\vec{\theta}) - d_i^{(Q)}}{\sigma_i^{(Q)}} \left[\Lambda^{-1}\right]_{ij} \frac{p_j^{(Q)}(\vec{\theta}) - d_j^{(Q)}}{\sigma_j^{(Q)}} \right\}, \qquad \text{(S.1)}$$

where $\sigma_i^{(Q)}$, with $Q = s, \chi_2^B$ represent error bars for the different points from lattice QCD.

$$\log \mathcal{L} = \frac{-1}{1-\Gamma^2} \left[(1+\Gamma^2)\,\zeta^2 - \Gamma\,\psi - \Gamma^2\,\phi \right] - (N-1)\,\log(1-\Gamma^2) + \text{const.}\,,$$

$$\zeta^2 \equiv \frac{1}{2} \sum_i \sum_{Q=s,\chi_2} \left(\frac{p_i^{(Q)}(\vec{\theta}) - d_i^{(Q)}}{\sigma_i^{(Q)}} \right)^2,$$

$$\psi \equiv \sum_i \sum_{Q=s,\chi_2} \frac{p_i^{(Q)}(\vec{\theta}) - d_i^{(Q)}}{\sigma_i^{(Q)}} \frac{p_{i+1}^{(Q)}(\vec{\theta}) - d_{i+1}^{(Q)}}{\sigma_{i+1}^{(Q)}},$$

$$\phi \equiv \frac{1}{2} \left[\left(\frac{p_1^{(Q)}(\vec{\theta}) - d_1^{(Q)}}{\sigma_1^{(Q)}} \right)^2 + \left(\frac{p_N^{(Q)}(\vec{\theta}) - d_N^{(Q)}}{\sigma_N^{(Q)}} \right)^2 \right].$$

Remarkably, the posterior 95% confidence interval obtained for the correlation strength is of $\Gamma = 0.84^{+0.03}_{-0.06}$, for both the PHA and PA models. This impressive agreement indicates that its value does not reflect the parametrization, but rather the lattice QCD error bars.

e-Print: 2309.00579 [nucl-th]

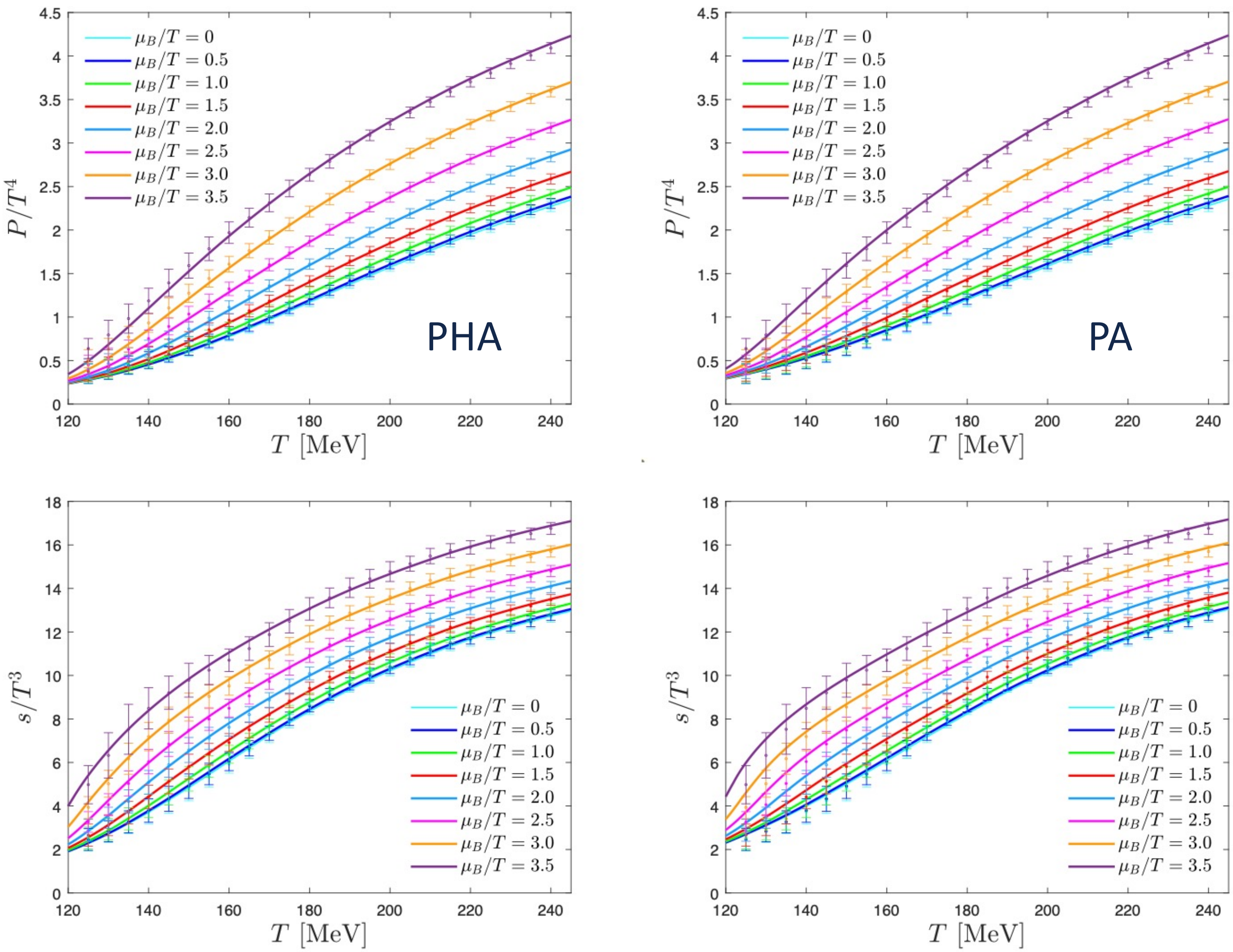

e-Print: 2309.00579 [nucl-th]

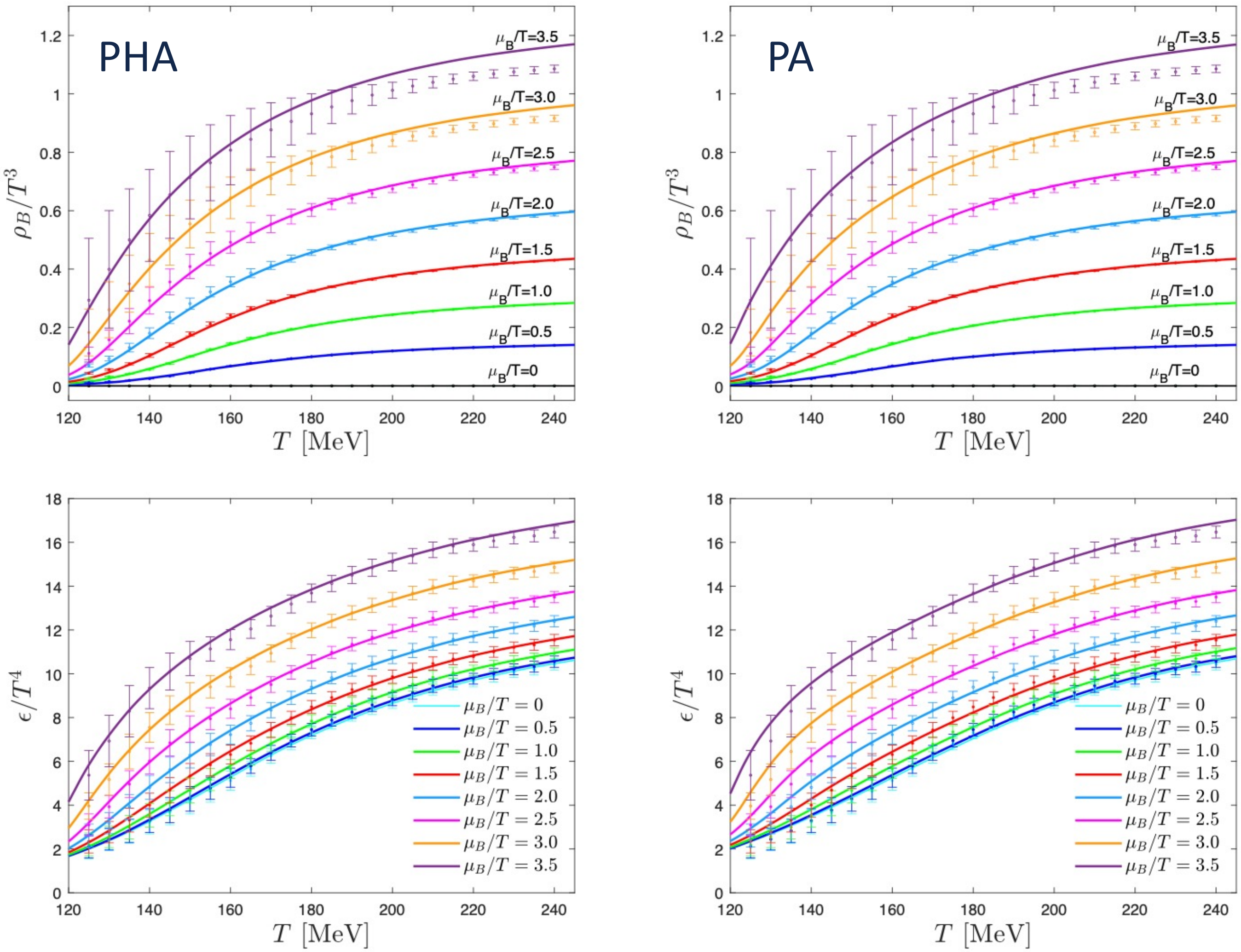

e-Print: 2309.00579 [nucl-th]

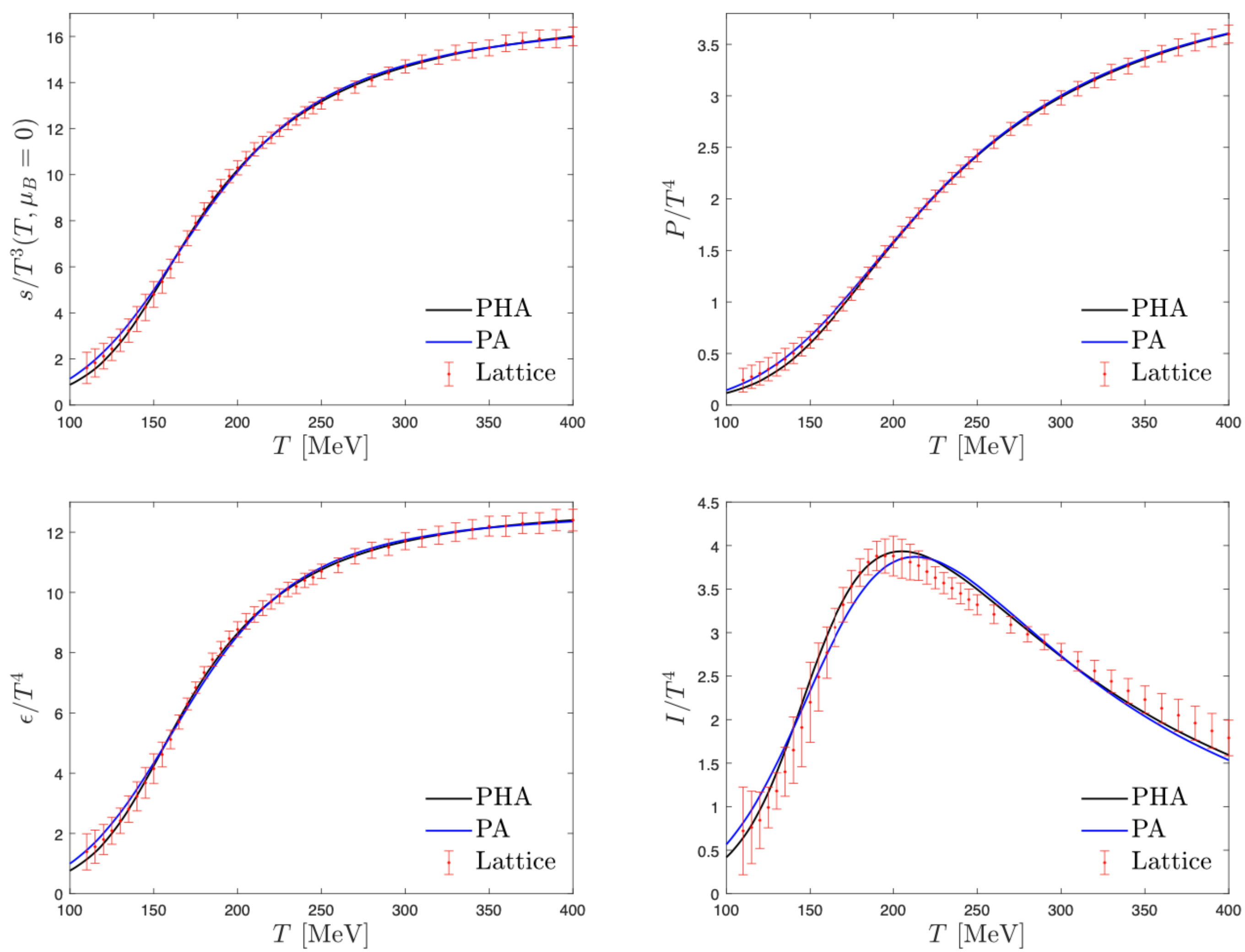

FIG. 8. Comparison between the best fit for the PHA and PA models and the lattice equation of state at zero chemical potential from Ref. [25]

Comparison to DBI action

From Jarvinen, and Piispa, 2405.02394v1 [hep-th], PRD (2024)

$$S_{\mathrm{DBI}} = \frac{1}{2\kappa_5^2}\int \mathrm{d}^5x \left\{\sqrt{-g}\left[R - \frac{1}{2}g^{\mu\nu}\partial_\mu\phi\partial_\nu\phi - V_{\mathrm{g}}(\phi)\right] - V_{\mathrm{f}}(\phi)\sqrt{-\det(g_{\mu\nu} + w(\phi)F_{\mu\nu})}\right\}$$

$$\Downarrow$$

$$S_{\mathrm{EMD}} = \frac{1}{2\kappa_5^2}\int \mathrm{d}^5x\sqrt{-g}\left[R - \frac{1}{2}g^{\mu\nu}\partial_\mu\phi\partial_\nu\phi - V(\phi) - \frac{Z(\phi)}{4}F_{\mu\nu}F^{\mu\nu}\right]$$

Mapping

$$V(\phi) = V_{\mathrm{g}}(\phi) + V_{\mathrm{f}}(\phi)\ , \qquad Z(\phi) = V_{\mathrm{f}}(\phi)w(\phi)^2\ , \qquad (\mu_{\mathrm{B}} \to 0)$$

Comparison to DBI action

From Jarvinen, and Piispa, 2405.02394v1 [hep-th], PRD (2024)

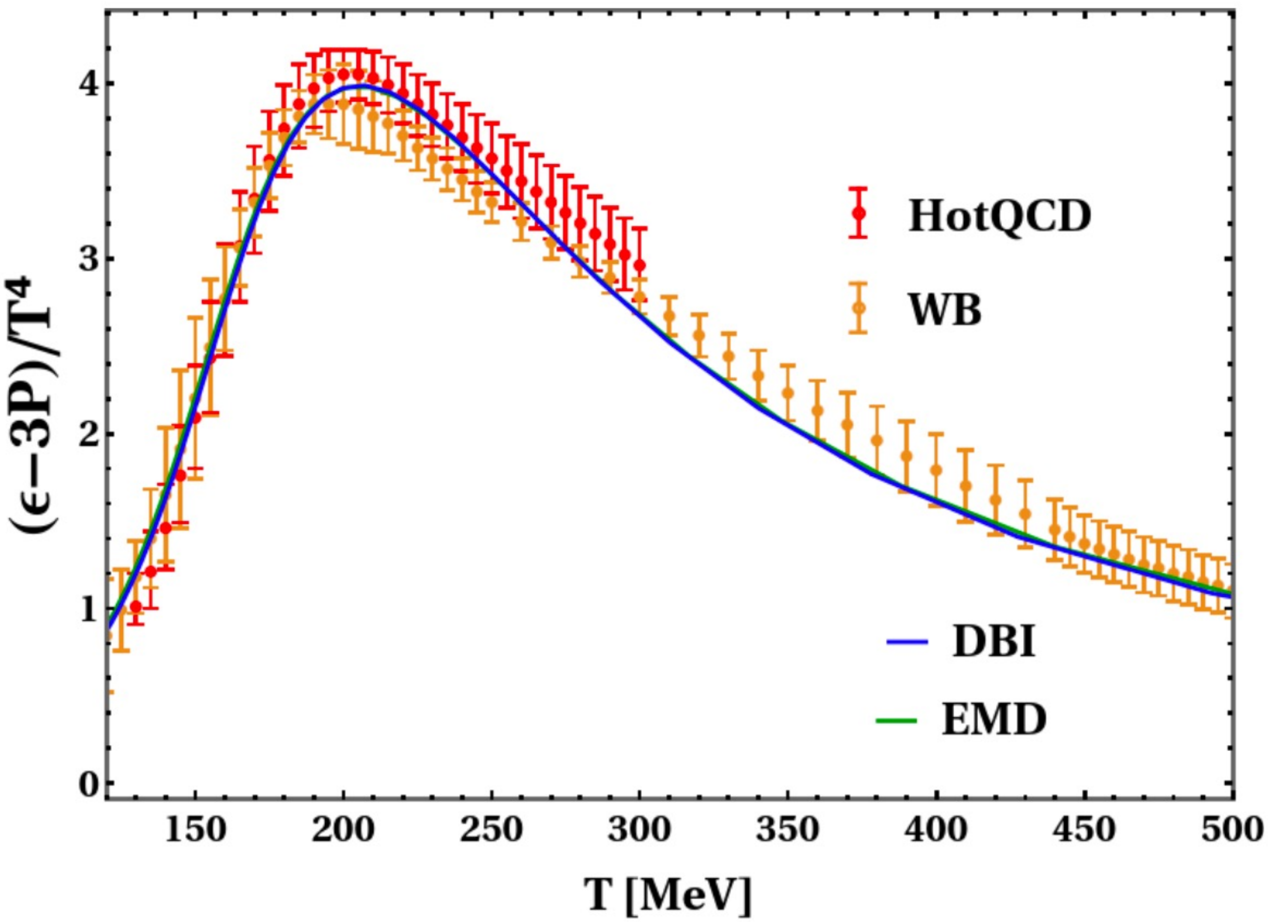

Comparison to DBI action

From Jarvinen, and Piispa, 2405.02394v1 [hep-th], PRD (2024)

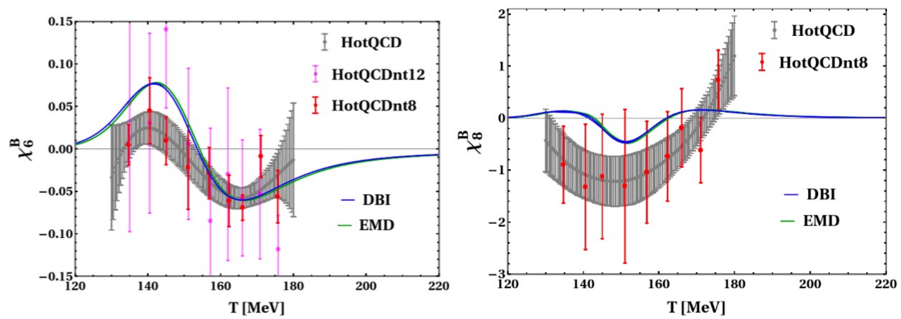

(a) (b)

Figure 5: **Left**: Sixth order susceptibility χ_6^B as a function of temperature at vanishing density. **Right**: Eight order susceptibility χ_8^B as a function of temperature at vanishing density. In both plots we display the results from both holographic models and the lattice data available from HotQCD collaboration [35]. The gray band is the continuum extrapolated value. Finite size lattice results are also shown.

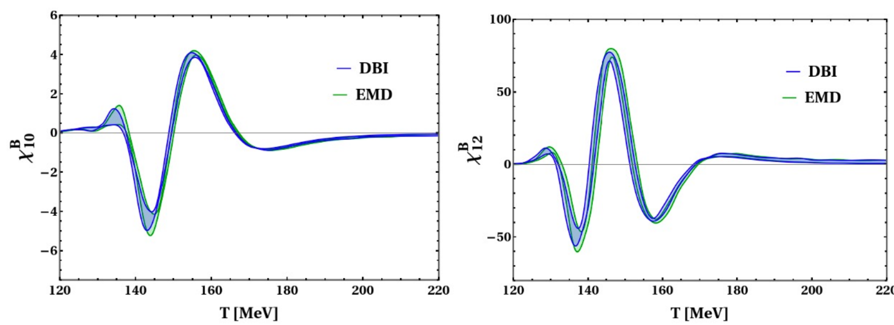

(a) (b)

Figure 6: **Left**: Tenth order susceptibility χ_{10}^B as a function of temperature at vanishing density. **Right**: Twelfth order susceptibility χ_{12}^B as a function of temperature at vanishing density.

Comparison to DBI action

From Jarvinen, and Piispa, 2405.02394v1 [hep-th], PRD (2024)

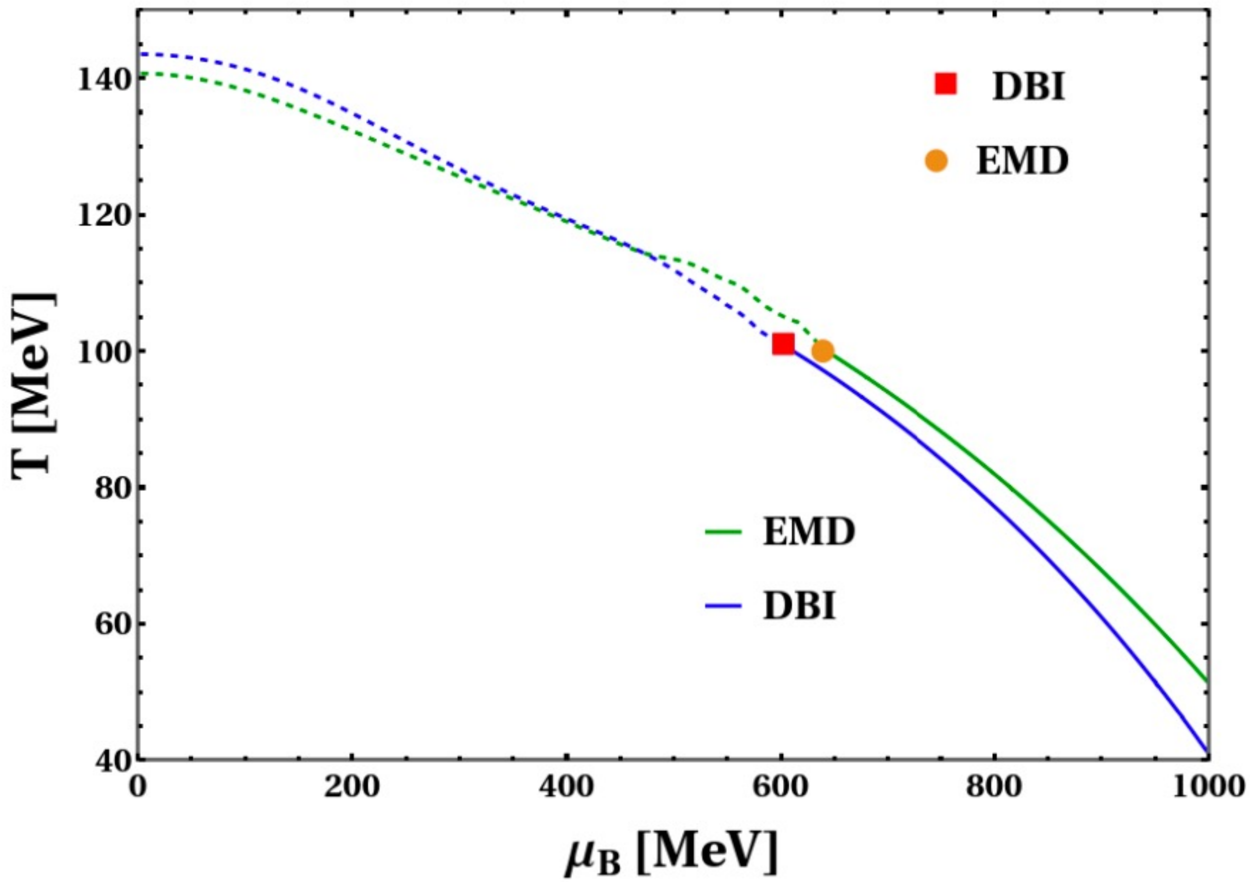

Comparison to DBI action

From Jarvinen, and Piispa, 2405.02394v1 [hep-th], PRD (2024)

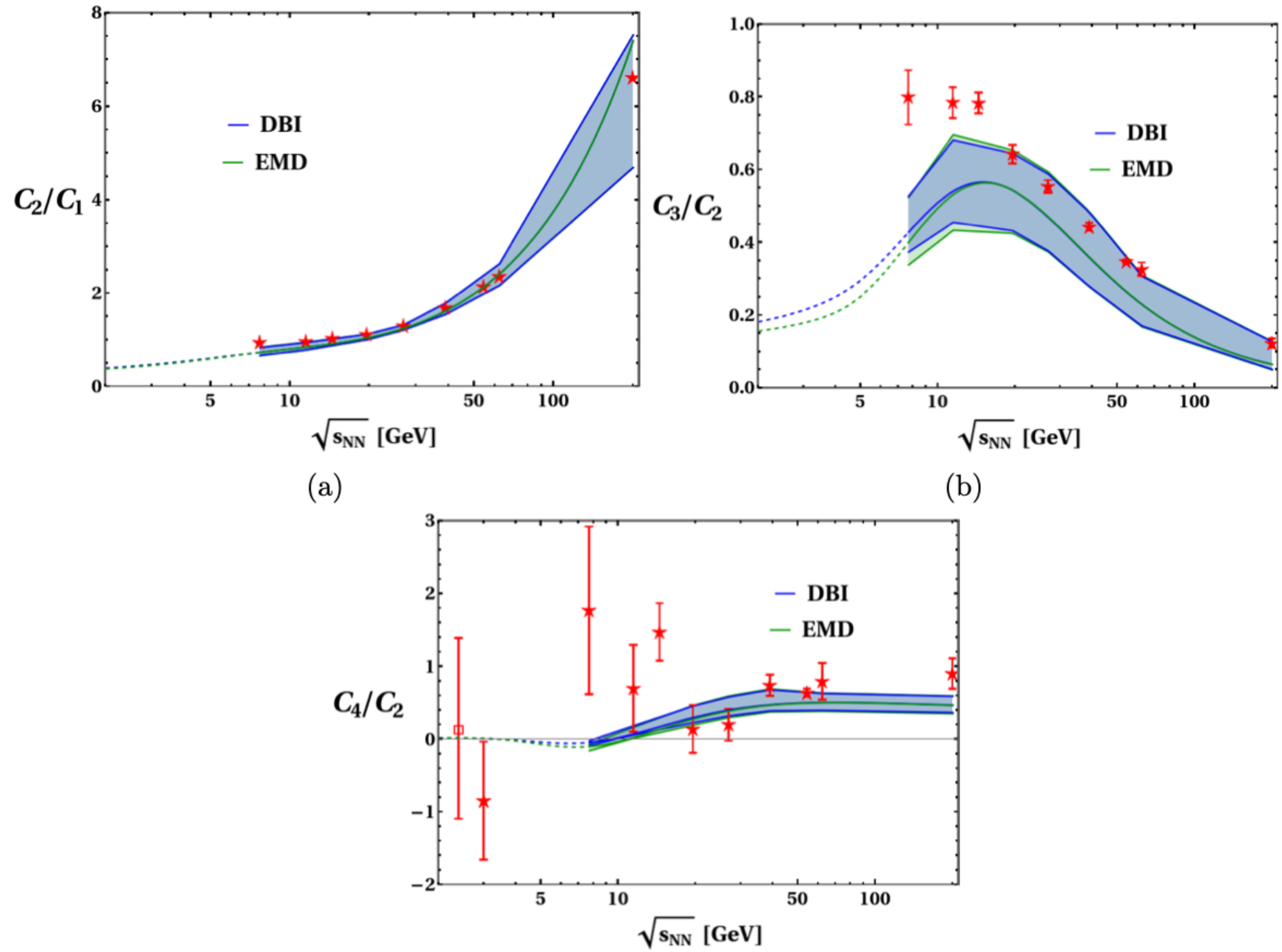

Chiral Condensate

Probe action (a la KKSS) + EMD model

From Fu et al, arXiv: 2404.12109 [hep-ph]

$$S_{X_q} = \frac{1}{2\kappa_N^2}\int d^5x\sqrt{-g}Z_q(\phi)\left[-\frac{1}{2}\nabla_\mu X_q \nabla^\mu X_q - V\left(X_q\right)\right] + S_{X_q,\partial}$$

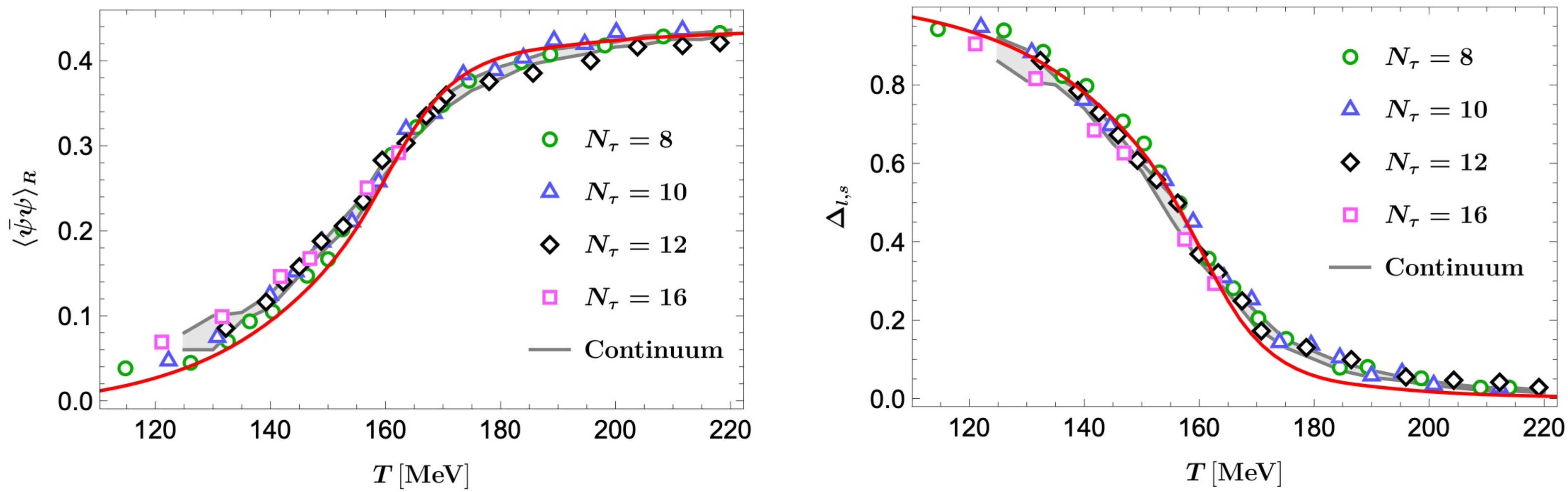

Figure 7: Renormalized chiral condensate and subtracted chiral condensate compare with lattice data [46].

Modular Unified Solver of the Equation of State collaboration

- Funded by NSF through CSSI program
- Developers and Users are working together to create a sustainable software to generate equations of state in the whole phase space
- Modular: Different models (``modules") to describe the EoS in different regimes of phase space
- Unified: Modules smoothly integrated to (i) ensure maximal coverage of phase space, and (ii) respects constraints

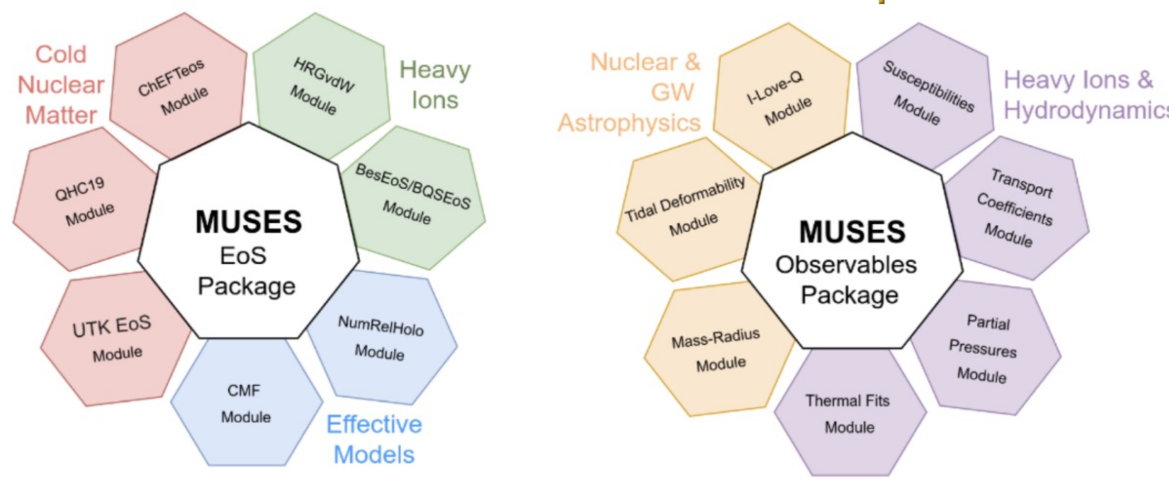

Join The Collaboration

- 21 institutions, 7 countries
- Synergistic collaboration between nuclear, astrophysics, gravitational wave, and computer science

Grefa et al, PRD, (2022)

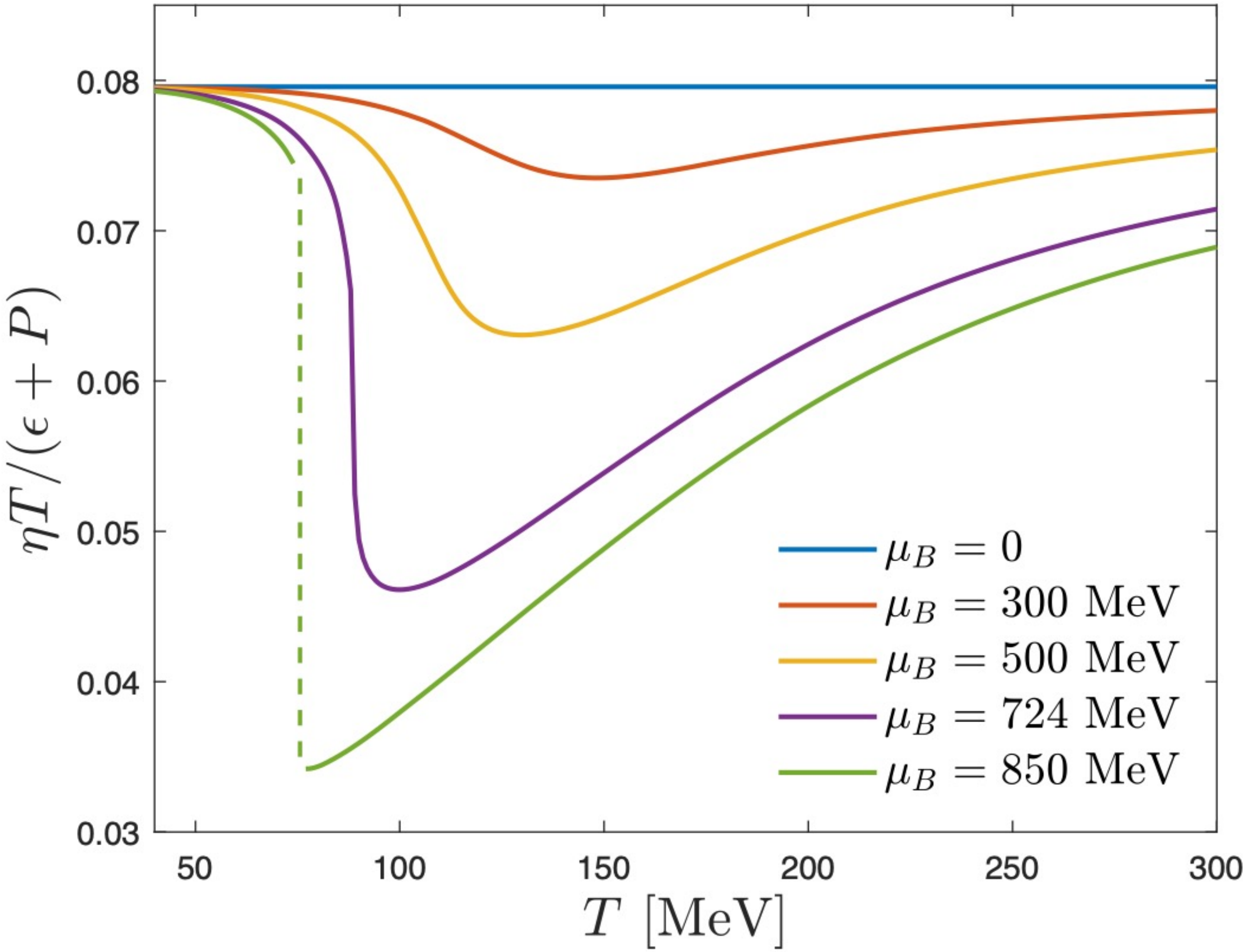

Grefa et al, PRD, (2022)

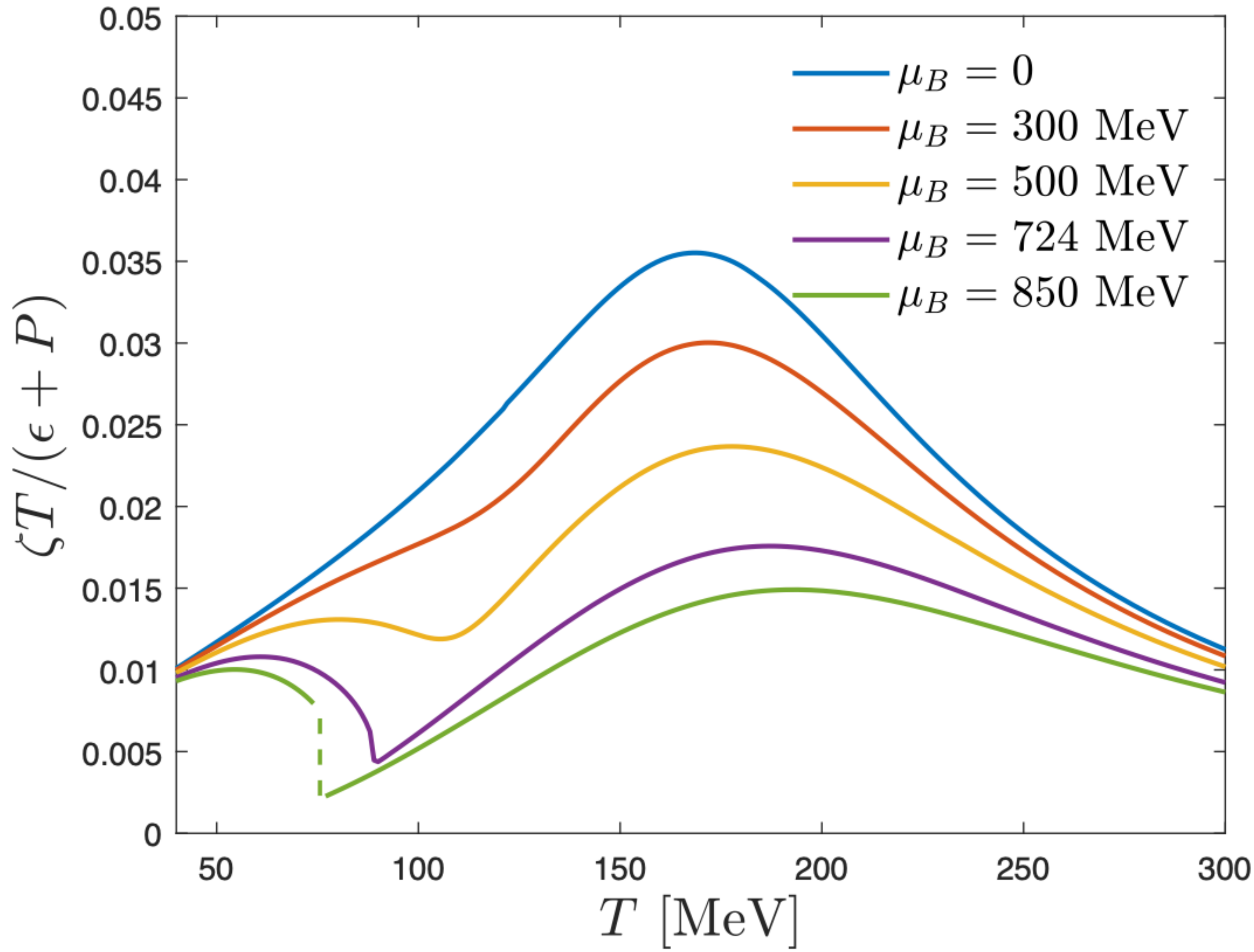

Grefa et al, PRD, (2022)

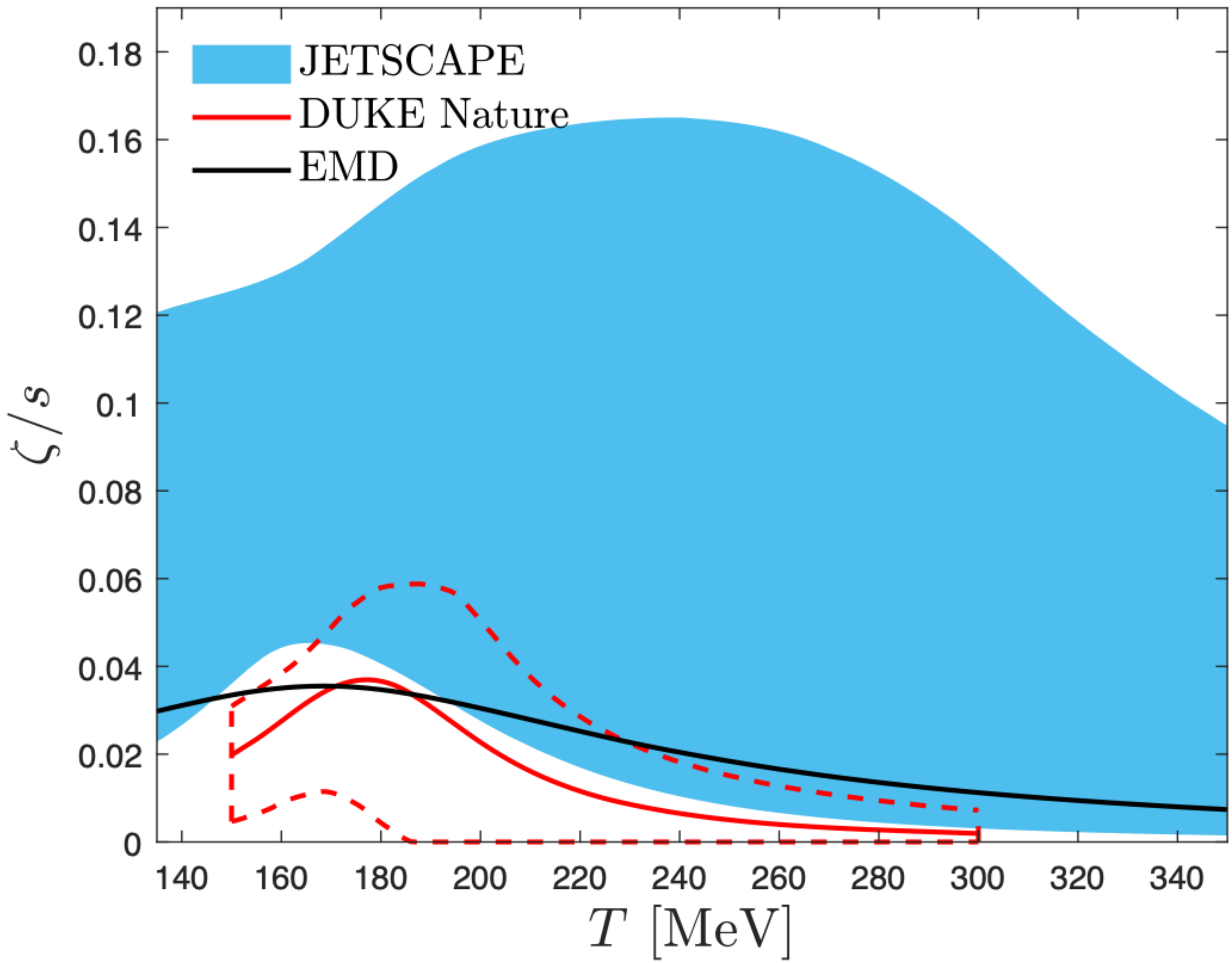

Grefa et al, PRD, (2022)

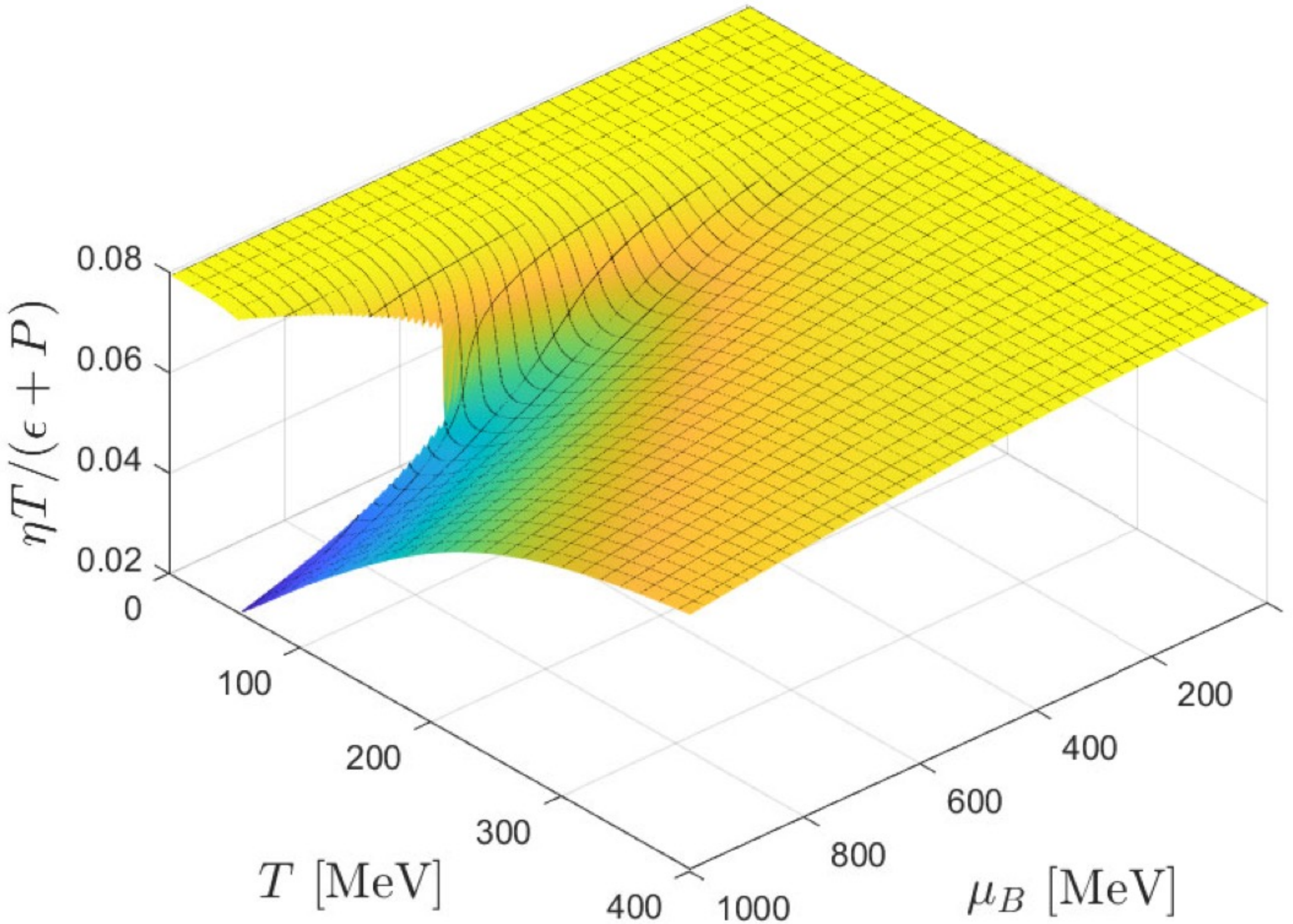

Grefa et al, PRD, (2022)